A COMPUTER VISION APPROACH TO ASSESS WOOD VARIABILITY FROM WHOLE-DISK IMAGES OF LONGLEAF PINE

by

SAMEEN RAUT

(Under the Direction of Joseph Dahlen)

ABSTRACT

This thesis investigated wood and fiber quality from planted longleaf pine. Eight forest cutover and eight old agriculture field stands were sampled, with a total of 160 trees felled per site type. Disks were collected from each tree at multiple height levels. In chapter 1, "Models to predict whole-disk specific gravity and moisture content in planted longleaf pine", non-linear mixed effects models were developed to predict the variation in wood and bark specific gravity (SG) with respect to relative height, age, and site type. Forest cutover sites had a higher whole-tree wood SG (0.504 vs 0.455) and bark SG (0.374 vs 0.347) than old agriculture field sites with the final wood and bark SG models explaining 50% and 37% of the variability, respectively. In chapter 2, "A computer vision approach to assess wood variability from whole-disk images of longleaf pine", disks were surfaced and imaged. Estimates from images were in close agreement with reference measurements for wood volume ($R^2 > 0.99$), bark volume ($R^2 = 0.96$), outside bark diameter ($R^2 > 0.99$) and inside bark diameter ($R^2 > 0.99$). Additional measurements of disk shape and compression wood were estimated from the disk images.

INDEX WORDS: compression wood, disk shape, moisture content, *Pinus palustris*, pith eccentricity, southern pine, specific gravity, wood and fiber quality, wood density

A COMPUTER VISION APPROACH TO ASSESS WOOD VARIABILITY FROM WHOLE-DISK IMAGES OF LONGLEAF PINE

by

SAMEEN RAUT

B.Sc., Tribhuvan University, Nepal, 2017

A Thesis Submitted to the Graduate Faculty of The University of Georgia in Partial Fulfillment of the Requirements for the Degree

MASTER OF SCIENCE

ATHENS, GEORGIA

2020

A COMPUTER VISION APPROACH TO ASSESS WOOD VARIABILITY FROM WHOLE-DISK IMAGES OF LONGLEAF PINE

by

SAMEEN RAUT

Major Professor:	Joseph Dahlen
Committee:	Bronson P. Bullock Cristián R. Montes

Electronic Version Approved:

Ron Walcott
Interim Dean of the Graduate School
The University of Georgia
August 2020

To my loved ones

ACKNOWLEDGEMENTS

The first person I would like to thank on this page is my major professor Dr. Joseph Dahlen who saw me worthy of the opportunity to take on this project and guided me all the way to its successful completion. I would like to thank the Natural Resources Conservation Service (NRCS) for funding this project and Dr. David Dickens for his key role in the project. I am thankful to my committee members Dr. Bronson Bullock and Dr. Cristián Montes for their input in helping me finish this project. I am grateful to Bryan Simmons from the Wood Quality Consortium (WQC) who was a key player during the field work for sample collection and lab work for sample processing. I am deeply appreciative of the help from my colleagues Thomas Harris and Mark Porter during the field work and Nawa Raj Pokhrel for helping me finish the lab work in time. I would like to thank the Plantation Management Research Cooperative (PMRC) field crew for their help in the final days of the field work. I would like to acknowledge landowners Ben O'Conner, Chuck Fore, David Wells, Georgia Power, Heather Brassel, Joseph W. Jones Ecological Research Center at Ichauway, Lynda Beam, Lamar Zipperer, Larry Hardy, Mark Dixon, Pete Peebles, Pete Studstill, and Rayonier for allowing sample collection from their planted longleaf pine stands. I must not forget to acknowledge my friends Dr. Suraj Upadhaya and Sagar Godar Chhetri who kept me motivated throughout this journey. I am indebted to my family members for their love and support.

TABLE OF CONTENTS

Page

LIST OF TABLES

Page

LIST OF FIGURES

Page

CHAPTER 1

MODELS TO PREDICT WHOLE-DISK SPECIFIC GRAVITY AND MOISTURE CONTENT IN PLANTED LONGLEAF PINE[1]

[1] Raut, S and Dahlen, J. To be submitted to [Canadian Journal of Forest Research]

ABSTRACT

Efforts to restore longleaf pine across the southeastern United States has occurred on two distinct plantation site types, forest cutover and old agricultural fields, the latter having higher residual nutrients from previous frequent fertilizer application. We assessed wood and bark physical properties of unthinned planted longleaf pine, ages 12 to 25, from sixteen stands across Georgia. A total of 320 trees were felled, with 3,572 cross-sectional disks collected from multiple height levels with wood and bark specific gravity (SG), moisture content (MC), and proportion of bark measured. Non-linear mixed effects models were developed to predict the variation in wood and bark SG with respect to relative height, age, and site type. Cutover sites had higher whole-tree wood SG (0.504 vs 0.455) and bark SG (0.374 vs 0.347) than old agriculture fields with the final wood and bark SG models explaining 50% and 37% of the variability, respectively. Moisture content also varied by site type with both wood MC ($R^2 = 0.86$) and bark MC ($R^2 = 0.69$) predicted as a function of SG. Bark dry mass and green volume were higher for cutover sites. These results provide important information to utilization of plantation longleaf pine.

Keywords: corewood and outerwood, forest cutover, juvenile and mature wood, old agriculture field, *Pinus palustris*, southern pine, wood and fiber quality, wood density.

1.1 INTRODUCTION

In the United States and worldwide, southern pine is one of the most commercially important species groups and it consists of loblolly pine (*Pinus taeda* L.), slash pine (*Pinus elliottii* Engelm.), longleaf pine (*Pinus palustris* Mill.), and shortleaf pine (*Pinus echinata* Mill.)) (Wear and Greis 2012). Today, loblolly pine is the most important southern pine since it has been extensively planted because of its fast growth (Schultz 1999; McKeand et al. 2003; Eberhardt et al. 2018). In the 19th and early 20th century, forests across the South were lost due to urbanization or converted to agriculture lands (VanLear et al. 2005). Prior to this land conversion, longleaf pine grew from southern Virginia to central Florida and into east Texas (Landers et al. 1995). Longleaf pine was the dominant tree species on 30 million hectares and was also found in mixed stands on 7 million hectares (Frost 1993). Today's dominant loblolly pine was largely found only on wet sites because of its poor tolerance to fire, which was a common practice (Schultz 1999).

Today, longleaf pine grows on approximately 2 million hectares (Oswalt et al. 2012; McIntyre et al. 2018). A major reason why longleaf pine was not replanted and instead planting of loblolly or slash pine occurred, is because longleaf pine has a grass stage to which the plant places emphasis on root development rather than on above ground stem growth (Brockway et al. 2005). As a result, early growth in longleaf pine is slower than the other southern pines (Cram et al. 2010; Dickens and Moorhead 2018). The grass stage lasts between 2 to 20 years depending upon factors including genetics, site quality, and forest management practices (Brockway et al. 2005; Dickens and Moorhead 2018). Haywood et al. (2015) report that planted longleaf pine in central Louisiana had transitioned from the grass stage towards the end of the fourth growing season. Cram et al. (2010) report that in South Carolina sandhill sites the grass stage lasted only 2 years. At the end of 10 growing seasons, planted longleaf pine lagged behind both loblolly and slash pines in terms of

height growth and total volume (Haywood et al. 2015). At age 15, Outcalt (1993) reported that longleaf pine outperformed loblolly and slash with greater height and diameter growth in sandhill sites of Georgia and South Carolina and concluded that longleaf pine is a suitable species for longer rotations.

Longleaf pine forest ecosystems contain many unique species (Brockway and Lewis 1997; Johnson and Gjerstad 2006) and because of this, there has been a push to restore longleaf pine. Beginning in 1995 and continuing through today, efforts by the Longleaf Alliance, America's Longleaf Restoration Initiative, and the Natural Resource Conservation Service (NRCS) Longleaf Pine Initiative have helped restore longleaf pine on private lands by providing technical assistance and financial incentives not available for other southern pines (Hainds 2004). Collectively these efforts have led to the establishment of nearly 400,000 additional hectares of longleaf pine throughout the southeastern U.S. (Oswalt et al. 2012).

One of the touted advantages to growing longleaf pine is that it is typically considered to be a low risk species and it has high wood quality relative to the other southern pines (Landers et al. 1995; Dickens et al. 2018). Wood specific gravity (SG) (wood density divided by the density of water) is one of the most important indicators of wood quality for the southern pines (Megraw 1985; Larson et al. 2011). Wood SG increases radially as cambial age increases (Mora et al. 2007; Jordan et al. 2008; Dahlen et al. 2018; Schimleck et al. 2018) due to thickening of the cell walls (Larson et al. 2001). Wood SG is positively correlated with mechanical properties (Antony et al. 2010) and Kraft pulp yield (Koch 1972). The Wood Handbook (Forest Products Laboratory 2010; Kretschmann 2010) lists average wood SG values at green moisture content (MC) for longleaf pine that are equivalent to slash pine (0.54) and higher than loblolly pine or shortleaf pine (0.47). The Wood Handbook (Kretschmann 2010) does not provide origin information on the samples,

however the samples were probably collected from naturally regenerated longleaf pine stands that were relatively old. Thus these SG values do not necessarily reflect longleaf pine growing in plantations, because said trees reach merchantable size much sooner than natural stands, and thus have a relatively high proportion of low SG corewood (juvenile wood) (Burdon et al. 2004; Mora et al. 2007; Moore and Cown 2017; Dahlen et al. 2018).

An additional factor that may influence the wood quality of longleaf pine has been that the re-establishment has occurred on two primary land site types, on forest cutover sites where the prior rotation was likely planted loblolly pine, slash pine, or natural longleaf pine, or on old agricultural fields where the prior crop was something other than a tree (Hainds 2004; Johnson and Gjerstad 2006; Kush et al. 2006). Old agriculture fields have different soil characteristics, with significantly more available nutrients available from repeated fertilizer applications, and essentially no hardwood competition through the first thinning as compared to cutover sites (Clabo et al. 2020). The abundant nutrients and low planting density of less than 1235 trees ha^{-1} (South 2006) result in a comparatively higher growth rate which could lower the SG compared to forest cutover sites (Clark et al. 2008). In loblolly pine and after accounting for cambial age differences, faster growth typically results in a subtle reduction in wood SG (Jordan et al. 2008; Dahlen et al. 2018). The lack of genetic improvement in longleaf pine combined with the rapid growth has also resulted in trees having a high amount of defects (Dickens et al. 2018). Dickens and Moorhead (2018) reported that some old field longleaf pine stands had over 50% stem defect rate with forking and ramicorn branches being the most common defects. The high defect rate will result in increased formation of low-quality compression wood. Compression wood has higher wood SG than normal or opposite wood, high lignin content, and has high longitudinal shrinkage resulting in lumber warp due to the high microfibril angles (Timell 1986; Nyström and Kline 2000; Sharma et al.

2017). Compression wood greatly reduces the suitability of trees to produce high quality pulp or dimension lumber (Nicholls 1982; Pont et al. 2007).

The longleaf pine that was planted in the early 2000s are beginning to be harvested, and thus there are questions about the suitability of the material and how it relates to the current perception of longleaf pine, that being slow growing and naturally regenerated longleaf pine. A significant amount of information is available on the wood and fiber quality of planted loblolly pine (Mora et al. 2007; Jordan et al. 2008; Antony et al. 2015; Dahlen et al. 2018; Schimleck et al. 2018), and to a lesser extent slash pine (Eberhardt et al. 2017), however there is little information available on the wood quality of planted longleaf pine following the recent restoration efforts where longleaf pine has been planted at lower planting densities (1235 trees ha^{-1}) (South 2006) compared to the past (2470 trees ha^{-1} to 3700 trees ha^{-1}) (Baldwin and Saucier 1983; Gibson et al. 1986). Bark properties are of interest to bioenergy facilities for bioproducts, and for burning for energy which is the conventional use of bark (Baker et al. 2012). Therefore, the objective of this study is to measure and model wood and bark SG and MC in planted longleaf pines grown in two specific site types (forest cutover and old agriculture field) from samples collected from unthinned stands. This study will inform forest landowners and wood using industries on the wood and fiber quality of planted longleaf pine.

1.2 MATERIALS AND METHODS

Trees Used in the Study

A total of 320 trees from 16 stands across south Georgia (Figure 1.1) were sampled in the summer of 2018. The ownership of the stands included private (N = 9), industrial (N = 5) and non-profit (N = 2) landowners. All the stands were planted and unthinned, between the ages of

Figure 1.1. Map of the stand locations.

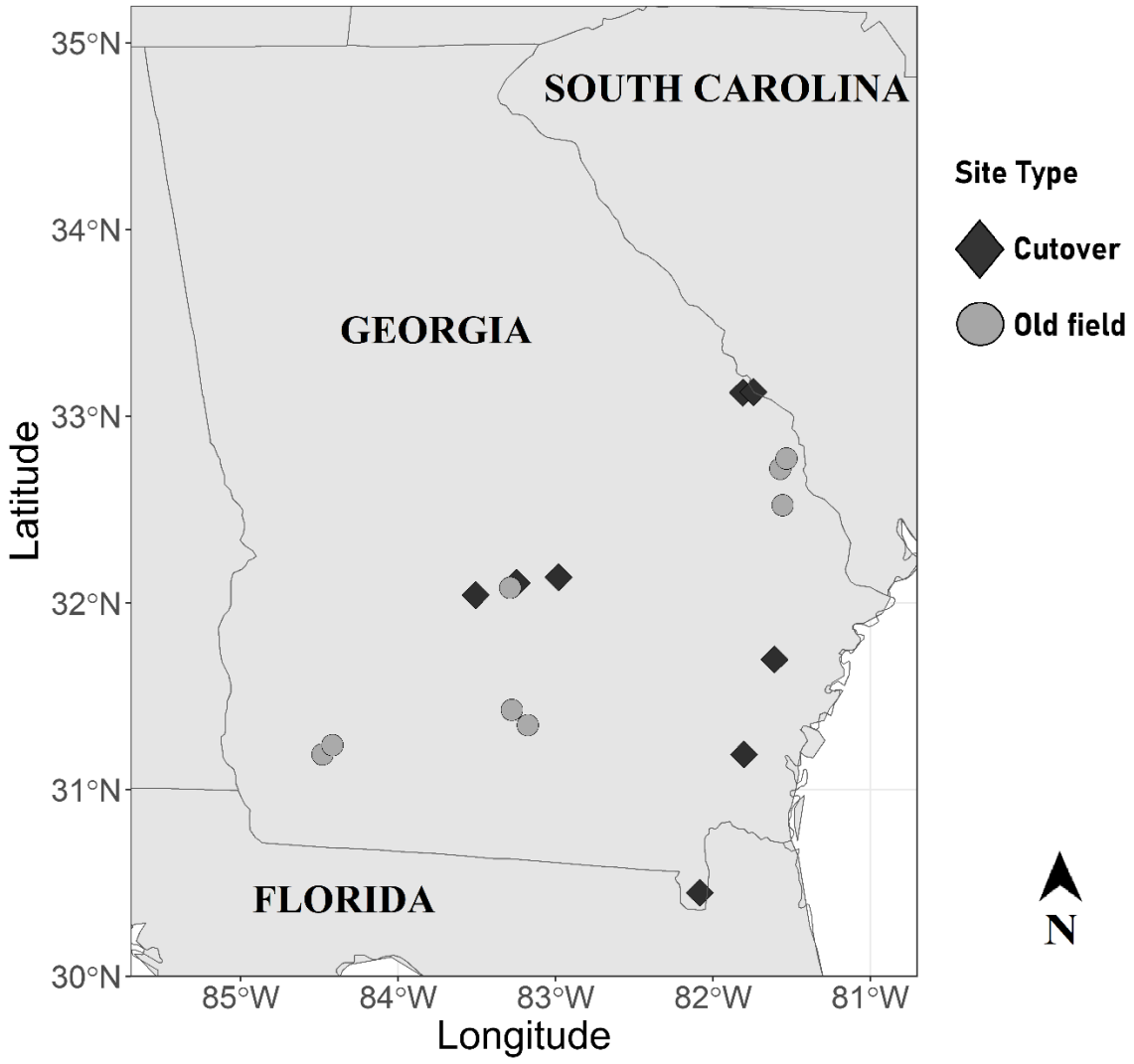

12 to 25 years old (mean age 17.2 years, standard deviation (SD) 3.7 years), and growing on two site types: either a cutover forest site (N = 8) or a converted agricultural field in the prior crop (old field) (N = 8). For the cutover stands, 4 were prescription burned once or multiple times, 3 were never burned, and 1 stand did not have prescription burning information available. For the old field sites, 5 were burned, and the remaining 3 stands did not have burning information available. The average planting density was 1360 trees ha^{-1} (SD = 300 trees ha^{-1}) with the planting density ranging from 960 trees ha^{-1} to 2150 trees ha^{-1}. For cutover sites, the mean planting density was 1350 trees ha^{-1} (SD = 424 trees ha^{-1}) and for old field sites the mean planting density was 1370 trees ha^{-1} (SD

= 80 trees ha^{-1}). The diameter distribution of each stand was obtained from cruise data by establishing three 0.0404 hectare sample plots in each stand. Twenty trees in each stand were selected and felled following the diameter distribution of the stand. Typically, wood and fiber quality studies focus on sampling only defect-free trees (Schimleck et al. 2019), however, due to the high proportion of longleaf pine with defects (Dickens and Moorhead 2018; Dickens et al. 2018), we also sampled trees with defects including forks, excessive sweep, ramicorn branches, and fusiform rust. From each stand, not more than 6 defect trees were sampled with the number determined based on the number of the defect trees measured during the inventory work. For the cutover sites a total of 25 defect trees were sampled and for old field sites a total of 31 defect trees were sampled. Table 1.1 shows the summary of the stands with location, age, site type, mean DBH, and mean total height.

Tree Sampling and Disk Measurements

Trees were felled using a chainsaw and delimbed. The total height of the main stem was measured using a logger's tape to one-tenth of a feet. Cross-sectional disks of approximately 5 cm thickness were collected at 0.15 m (stump height), 0.6 m, 1.37 m (breast height), 2.44 m from the base and then at every 1.22 m intervals up to an outside bark diameter of 7.6 cm. For the forked trees, cross-sectional disks were collected at the same heights from the base as the other trees up to the crotch base. One disk was taken at the crotch base, one from the base of each of the forks and one at the 7.6 cm top from both the forks. When the fixed disk height overlapped branch whorls, the height was adjusted and the exact height recorded. A total of 3,572 cross-sectional disks were sampled for this study, placed in individual plastic bags, and transported back to the Wood and Fiber Quality Laboratory at the University of Georgia in Athens, GA, USA and frozen until sample processing began.

Table 1.1. General characteristics of the longleaf pine stands sampled with their locations.

Stand	Latitude	Longitude	Age (years)	Site type	DBH (cm)		Height (m)	
					Mean	SD	Mean	SD
1	32.1086	-83.2476	12	Cutover	15.2	2.1	12.2	0.9
2	32.0431	-83.5077	12	Cutover	15.6	2.5	10.5	1.1
3	33.1279	-81.7293	16	Cutover	16.2	2.6	13.5	1.2
4	32.1386	-82.9812	16	Cutover	16.7	3.2	13.3	1.2
5	33.1308	-81.7435	19	Cutover	17.5	3.4	16.1	1.7
6	31.1896	-81.8029	19	Cutover	18.1	3.5	17.8	1.9
7	31.6985	-81.6093	22	Cutover	20.6	4.4	20.1	1.4
8	30.4488	-82.0834	25	Cutover	16.9	3.0	15.5	1.3
9	32.0823	-83.2877	12	Oldfield	18.5	2.9	12.9	0.9
10	32.5242	-81.5562	14	Oldfield	16.0	3.0	11.6	0.9
11	31.4278	-83.2774	15	Oldfield	17.7	3.0	15.3	0.9
12	31.1893	-84.4805	17	Oldfield	22.3	3.2	17.1	0.9
13	31.2393	-84.4166	18	Oldfield	19.9	3.8	14.6	1.3
14	32.7196	-81.5711	19	Oldfield	20.8	3.9	16.1	1.1
15	32.7741	-81.533	19	Oldfield	20.9	5.0	15.8	1.3
16	31.346	-83.1759	20	Oldfield	20.5	3.4	15.5	1.1

Site Type	DBH (cm)				Height (m)			
	Mean	SD	Min	Max	Mean	SD	Min	Max
Cutover	17.4	3.7	10.2	29.2	15.4	3.3	8.1	22.5
Old field	19.7	4.0	9.9	30.5	15.0	1.9	9.8	18.7
Overall	18.6	4.0	9.9	30.5	15.2	2.7	8.1	22.5

Outside bark diameters of the disks were measured using a diameter tape. Green weight was measured using a digital scale. Bark was peeled off the green disks and then the inside bark diameters were measured. Double bark thickness was calculated as the difference of outside and inside bark diameters. Green weight of the wood was measured after bark removal and the difference between green weight of the unpeeled and peeled disks gave the total green weight of bark. The largest piece of bark (having intact inner and outer bark) from each disk was weighed, and the wood disk and the bark section soaked in water for 48-72 hours. Green volume of the largest bark pieces and wood disks were measured using water displacement (ASTM International 2017). The bark pieces and the disks were then oven dried at 103 ± 2ºC until the weight stabilized and then the oven dry weights were recorded using a digital scale. Wood and bark SG and MC were then calculated:

$$\mathrm{SG} = \frac{\mathrm{Weight_{OD}}}{\mathrm{Volume}} \times \frac{1}{\mathrm{K}} \quad (1)$$

where, SG is the basic specific gravity of the material, $\mathrm{Weight_{OD}}$ is the oven-dry weight (in grams) of that material, Volume is the green volume (in $\mathrm{cm^3}$) of that material and K is the density of water (1 g $\mathrm{cm^{-3}}$). Moisture content was calculated as:

$$\mathrm{MC} = \frac{\mathrm{Weight_G} - \mathrm{Weight_{OD}}}{\mathrm{Weight_{OD}}} \times 100 \quad (2)$$

where, MC is the moisture content of the material in percentage, $\mathrm{Weight_G}$ is the green weight (in grams), and $\mathrm{Weight_{OD}}$ is the oven-dry weight (in grams).

Statistical Analysis and Model Fitting

Given the type of data, a mixed effect analysis was selected as the test for the hypothesis. All statistical analyses and graphics were done in R statistical software (R Core Team 2020) using

the RStudio Interface (RStudio 2020). Packages used were ggplot2 (Wickham 2016), maps (Becker et al. 2018), needs (Katz 2016), nlme (Pinheiro et al. 2018), plyr (Wickham 2011), rgeos (Bivand and Rundel 2019), rnaturalearth (South 2017), rnaturalearthdata (South 2017), and sf (Pebesma 2018). Whole-tree wood and bark values were obtained by calculating the average of individual disks from a tree weighted by wood and bark surface area of those disks, relative to the total area for all the disks from a particular tree. The SG, MC, and green mass were calculated for wood. The SG, MC, green mass, dry mass, and double bark thickness were calculated for bark. For all the wood and bark variables, mean, standard deviation, minimum, and maximum values were calculated. Analysis of variance (ANOVA) using nonlinear mixed effects models with stands and trees sampled as random factors was done to test for differences in wood and bark SG and MC between cutover and old field sites. Linear and nonlinear models were fitted to explain the trends in dependent variables with respect to independent variables. Models were examined for their form using plots and compared based on their coefficient of determination (R^2) of the fixed and random (stand, tree) effects, Akaike Information Criterion (AIC) values, likelihood ratio tests, and root mean square error (RMSE).

Wood Specific Gravity Model Development

A three parameter nonlinear model from Ratkowsky (1990) was chosen for predicting the trend in wood SG (SGWood) with respect to relative height. Here the base wood SG model was:

$$\mathrm{SGWood}_{ijk} = (\beta_0 + \mathrm{b}_{0i} + \mathrm{b}_{0ij}) - \beta_1 \times \log\left(\mathrm{RHeight}_{\mathrm{ijk}} + \beta_2\right) + \varepsilon \qquad (3)$$

where, SGWood_{ijk} and $\mathrm{RHeight}_{ijk}$ are the wood SG and relative height of the *k*th disk from the *j*th tree in the *i*th stand, respectively. β_0, β_1, and β_2 are the fixed effects parameters, the nested random effects of the asymptote β_0 at the stand and tree levels are represented by b_{0i} and b_{0ij}, respectively,

and ε is the error term. Because SG increases with cambial age (Megraw 1985), the effect of age on wood SG was incorporated into the model as:

$$\mathrm{SGWood}_{ijk} = (\beta_0 + \mathrm{b}_{0i} + \mathrm{b}_{0ij}) - \beta_1 \times \log(\mathrm{RHeight}_{ijk} + \beta_2) + \beta_3 \times \mathrm{AGE}_i + \varepsilon \qquad (4)$$

where, β_3 is the added fixed effect regression parameter which explains the effect of age on wood SG and AGE_i is the age of the *i*th stand. Wood SG appeared to increase linearly with age for these samples. The other parameters are the same as equation (3).

One of the main objectives of this study was to determine the impact of site type on wood SG and therefore, this effect was incorporated into the model:

$$\mathrm{SGWood}_{ijk} = (\beta_0 + \mathrm{b}_{0i} + \mathrm{b}_{0ij}) - \beta_1 \times \log(\mathrm{RHeight}_{ijk} + \beta_2) + \beta_3 \times \mathrm{AGE}_i + \beta_4 \times \mathrm{SITETYPE}_i + \varepsilon \quad (5)$$

where, β_4 is the added fixed effect regression parameter to explain the effect of the type of site where the trees are grown on wood SG, $\mathrm{SITETYPE}_i$ specifies whether the *i*th stand is an old field site ($\mathrm{SITETYPE}_i$ = 1) or a cutover site ($\mathrm{SITETYPE}_i$ = 0). The other parameters are same as equation (4).

Reaction wood in softwood species that have defects such as sweep is seen in the form of compression wood which has noticeably higher wood SG than normal or opposite wood (Timell 1986; Sharma et al. 2017). Therefore, the effect of the defects on the wood SG was also incorporated into the model to give:

$$\mathrm{SGWood}_{ijk} = (\beta_0 + \mathrm{b}_{0i} + \mathrm{b}_{0ij}) - \beta_1 \times \log(\mathrm{RHeight}_{ijk} + \beta_2) + \beta_3 \times \mathrm{AGE}_i + \beta_4 \times \mathrm{SITETYPE}_i + \beta_5 \times \mathrm{DEFECT}_{ij} + \varepsilon \quad (6)$$

where, β_5 is the fixed effect regression parameter added to explain the effect of defects on wood SG. DEFECT_{ij} defines whether the *j*th tree in the *i*th stand has a defect (DEFECT = 1) or not (DEFECT = 0). The other parameters are the same as equation (5).

Wood Moisture Content Model Development

Rather than fitting wood MC as a function of relative height, we fitted wood MC as a function of wood SG. Within a species, higher SG wood tends to have lower MC (Antony et al. 2015; Eberhardt et al. 2017; Dahlen et al. 2020b). The model was adapted from Ratkowsky (1990), the model for wood MC was:

$$\mathrm{MCWood} = \beta_0 \times \log(-\beta_1) + \beta_0 \times \ln(\mathrm{SGWood}) + \varepsilon \quad (7)$$

where, MCWood is the MC for the wood calculated from the SG of the wood (SGWood), ln is the natural logarithm, β_0 and β_1 are the regression parameters, and ε is the error term.

Bark Specific Gravity Model Development

To predict the trend in the data for bark SG with respect to relative height, a three-parameter nonlinear model used by Eberhardt et al. (2017) and adapted from Ratkowsky (1990) was used. The base bark SG model was:

$$\mathrm{SGBark}_{ijk} = (\beta_0 + \mathrm{b}_{0i} + \mathrm{b}_{0ij}) + \beta_1 \times \ln\left(\mathrm{RHeight}_{ijk}{}^{-\beta_2} - 1\right) + \varepsilon \quad (8)$$

where, SGBark_{ijk} and $\mathrm{RHeight}_{ijk}$ are the bark SG and relative height of the *k*th disk from the *j*th tree in the *i*th stand, respectively. β_0, β_1, and β_2 are the fixed effects parameters. Nested random effects of the asymptote β_0 at the stand and tree levels are represented by b_{0i} and b_{0ij}, respectively, and ε is the error term. Incorporating the effect of age on bark SG, the model was:

$$\mathrm{SGBark}_{ijk} = (\beta_0 + \mathrm{b}_{0i} + \mathrm{b}_{0ij}) + \beta_1 \times \ln\left(\mathrm{RHeight}_{ijk}{}^{-\beta_2} - 1\right) + \beta_3 \times \mathrm{AGE}_i + \varepsilon \quad (9)$$

where, β_3 is the added fixed effect parameter to explain the effects of age on bark SG and AGE_i is the given age of the *i*th stand, the other parameters are the same as equation (8). To determine if

the site type has any effect on longleaf pine bark SG, a site type term was incorporated into equation (9) to give the model:

$$\mathrm{SGBark}_{ijk} = \left(\beta_0 + \mathrm{b}_{0i} + \mathrm{b}_{0ij}\right) + \beta_1 \times \ln\left(\mathrm{RHeight}_{ijk}{}^{-\beta_2} - 1\right) + \beta_3 \times \mathrm{AGE}_i + \beta_4 \times \mathrm{SITETYPE}_i + \varepsilon \quad (10)$$

where, β_4 is the added fixed effect regression parameter to explain the effects of the type of site where the trees are grown on bark SG, $\mathrm{SITETYPE}_i$ represents either an old field site ($\mathrm{SITETYPE}_i = 1$) or a cutover site ($\mathrm{SITETYPE}_i = 0$). The other parameters are the same as equation (9). Trees affected by defects such as sweep show asymmetry in the cross sectional samples which can be explained by reaction wood development, however changes in bark are not noted in the literature and thus were not explored here (Scurfield 1973).

Bark Moisture Content Model Development

A similar approach to modeling wood MC was done for modeling bark MC where bark MC is deemed a function of bark SG. Using a model adapted from Ratkowsky (1990), the model for bark MC was:

$$\mathrm{MCBark} = \frac{1}{\beta_0 + \beta_1 \times \mathrm{SGBark} + \beta_2 \times \mathrm{SGBark}^2} + \varepsilon \quad (11)$$

where, MCBark is the MC for the bark based on the SG of the bark (SGBark). β_0, β_1, and β_2 are the regression parameters, and ε is the error term.

Diameter Outside Bark : Diameter Inside Bark Model Fitting

We found that cutover sites and old field sites had slightly different bark diameter ratios, as such, a simple linear model with no intercept but having a slope term was used to fit DIB with

respect to DOB separately for both cutover and old field sites. Hence, the diameter outside bark can be converted to diameter inside bark using:

$$\mathrm{DIB} = \beta_1 \times \mathrm{DOB} + \varepsilon \quad (12)$$

where, DIB is the inside bark diameter at a height in the tree where the outside bark diameter is DOB, β_1 is the regression parameter which was fit separately by site type, and ε is the error term.

1.3 RESULTS

Whole-Tree Wood Specific Gravity and Moisture Content

The overall average whole-tree wood SG for this study was 0.480 (SD = 0.046) with the values ranging from 0.376 to 0.620 (Table 1.2). Trees grown on cutover sites had a higher wood SG (Mean = 0.504, SD = 0.041) than trees grown on old field sites (Mean = 0.455, SD = 0.035) (p-value = 0.0013). The minimum whole-tree SG for both site types was the same (0.376), while the maximum SG for cutover sites (0.620) was much higher than old field sites (0.533). Seven out of the eight cutover stands had higher average whole-tree wood SG values than any of the old field stands, irrespective of age (Table 1.3). For a given site type, generally as stand age increased there was a gradual increase in wood SG with a few exceptions. For the cutover sites, stand 3 (aged 16 years) had higher average wood SG value (0.506 vs 0.485) than stand 5 (aged 19 years), and for old field sites, stand 11 (aged 15 years) had higher average wood SG value (0.458 vs 0.442) than stand 14 (aged 19 years). Thus, age was not the only factor driving wood SG differences in those stands.

The mean whole-tree wood MC for the study was 113% (SD = 20%) (Table 1.2) with the lowest whole-tree wood MC of 69% from one of the cutover sites, and the maximum value of

172% from an old field site. There was a significant difference in wood MC values among longleaf pine trees grown on cutover and old field sites (p-value = 0.0068). The mean whole-tree wood MC for cutover sites was 104% (SD = 17%) and that for old field sites was 123% (SD = 17%).

Table 1.2. Whole-tree wood and bark properties for longleaf pine in cutover and old field sites.

Tissue	Property	Overall (N= 320)				Cutover (N=160)				Old Field (N=160)				*P*-value
		Mean	SD	Min	Max	Mean	SD	Min	Max	Mean	SD	Min	Max	
Wood	Specific gravity	0.480	0.046	0.376	0.620	0.504	0.041	0.424	0.620	0.455	0.035	0.376	0.533	0.0013
	Moisture content[1]	113	20	69	172	104	17	69	141	123	17	86	172	0.0068
	Green mass[2]	1016	35	864	1088	1022	27	929	1081	1011	40	864	1088	0.3429
Bark	Specific gravity	0.360	0.035	0.254	0.519	0.374	0.026	0.306	0.460	0.347	0.037	0.254	0.519	0.0215
	Moisture content[1]	93	23	43	173	82	18	43	136	105	22	50	173	0.0034
	Green mass[2]	691	57	501	841	677	59	501	797	704	53	553	841	0.0986
	Dry mass[1]	17.8	3.8	8.8	33.0	19.4	3.7	11.5	33.0	16.1	3.1	8.8	29.3	0.0127
	Green volume[1]	22.3	4.5	12.8	42.7	24.4	4.6	14.7	42.7	20.1	3.2	12.8	27.8	0.0061
	Double bark thickness[3]	2.02	0.42	1.05	4.24	2.08	0.45	1.17	4.24	1.96	0.38	1.05	3.19	0.2094
Wood and Bark	Green mass of wood and bark to volume wood[2]	1216	64	1011	1417	1242	62	1101	1417	1189	55	1011	1310	0.0274
	Green mass of wood and bark to volume wood and bark[2]	942	37	783	1013	936	35	812	998	948	38	783	1013	0.3227

[1] %
[2] kg m^{-3}
[3] cm

Table 1.3. Stand level wood and bark properties for cutover and old field sites.

			Wood			Bark						Wood and Bark	
Stand	**Site type**	**Age**	**SG**	**MC[1]**	**Green mass[2]**	**SG**	**MC[1]**	**Green mass[2]**	**Dry mass[1]**	**Green volume[1]**	**Double bark thickness[3]**	**Wood and bark mass to wood volume[2]**	**Wood and bark mass to volume[2]**
1	Cutover	12	0.468	123	1043	0.367	94	713	20.6	24.9	2.02	1279	961
2	Cutover	12	0.484	116	1048	0.373	91	710	22.2	27.0	2.33	1311	956
3	Cutover	16	0.506	100	1012	0.368	86	685	19.6	25.2	2.24	1242	929
4	Cutover	16	0.481	114	1028	0.364	85	674	20.0	24.8	2.22	1250	940
5	Cutover	19	0.485	112	1028	0.370	88	696	17.2	21.4	2.01	1218	957
6	Cutover	19	0.520	96	1019	0.392	76	688	16.2	20.5	1.95	1196	951
7	Cutover	22	0.507	101	1020	0.390	74	679	15.0	18.7	2.01	1175	956
8	Cutover	25	0.547	85	1013	0.386	60	617	21.3	27.7	2.72	1250	903
9	Oldfield	12	0.438	132	1014	0.362	106	746	19.7	22.9	2.25	1236	953
10	Oldfield	14	0.412	150	1028	0.292	134	683	16.9	22.3	1.88	1224	952
11	Oldfield	15	0.458	123	1021	0.383	96	752	17.4	20.1	1.88	1210	967
12	Oldfield	17	0.462	125	1039	0.340	109	713	13.1	17.0	2.00	1185	984
13	Oldfield	18	0.471	120	1035	0.337	113	717	14.1	18.7	2.05	1200	976
14	Oldfield	19	0.442	114	945	0.370	89	698	15.2	17.7	2.02	1095	901
15	Oldfield	19	0.475	113	1011	0.368	85	681	16.4	20.2	2.25	1184	944
16	Oldfield	20	0.474	120	1044	0.338	97	667	14.7	19.4	2.19	1205	971

[1] %
[2] $kg\ m^{-3}$
[3] cm

Whole-Tree Bark Specific Gravity and Moisture Content

The average whole-tree bark SG was 0.360 (SD = 0.035) with a range from 0.254 to 0.519. Trees in cutover sites had a mean bark SG of 0.374 (SD = 0.026) whereas those in old field sites had a mean bark SG of 0.347 (SD = 0.037) and the difference was significant (p-value = 0.00215) as shown in Table 1.2. The average whole-tree bark MC was 93% (SD = 23%) with the lowest whole-tree bark MC value at 43% for a tree from one of the cutover sites and the maximum whole-tree bark MC value at 173% for a tree from one of the old field sites (Table 1.2). There was a significant difference in bark MC values of trees from cutover (Mean = 82%, SD = 18%) and old field (Mean = 105%, SD = 22%) sites (p-value = 0.0034).

Whole-Tree Green Weights of Wood and Bark

Whole-tree wood and bark green masses, and bark dry masses, green volumes, and double bark thicknesses were calculated (Tables 1.2 and 1.3). Also included were green mass of wood and bark to volume wood and green mass of wood and bark to volume wood and bark calculations. Whole-tree wood green mass yield was higher for cutover sites (Mean = 1022 $kg.m^{-3}$, SD = 27 $kg.m^{-3}$) as compared to that from old field sites (Mean = 1011 $kg.m^{-3}$, SD = 40 $kg.m^{-3}$), however, the difference was not statistically significant (p-value = 0.3429). Trees harvested from old field sites yielded more green mass of bark (Mean = 704 $kg.m^{-3}$, SD = 53 $kg.m^{-3}$) on average as compared to those from cutover sites (Mean = 677 $kg.m^{-3}$, SD = 59 $kg.m^{-3}$) though the difference was not significant (p-value = 0.0986). However, cutover sites (Mean = 19.4%, SD = 3.7%) had significantly higher amounts of dry bark yield than old field sites (Mean = 16.1%, SD = 3.1%) (p-value = 0.0127). The difference here being that old field sites had higher bark MC than cutover

sites. Cutover sites also had significantly higher bark green volumes (Mean = 24.4%, SD = 4.6%) as compared to old field sites (Mean = 20.1%, SD = 3.2%) (p-value = 0.0061), with greater double bark thickness (Mean = 2.08 cm, SD = 0.45 cm vs Mean = 1.96 cm, SD = 0.38 cm) although the difference in double bark thickness was not significant (p-value = 0.2094). For a given volume of wood, wood and bark from longleaf pine trees harvested from cutover sites yielded significantly more green mass (Mean = 1242 $kg.m^{-3}$, SD = 62 $kg.m^{-3}$) on average than old field sites (Mean = 1189 $kg.m^{-3}$, SD = 55 $kg.m^{-3}$) (p-value = 0.0274). However, for a given volume of wood and bark combined, wood and bark from longleaf pine trees harvested from old field sites yielded more green mass (Mean = 948 $kg.m^{-3}$, SD = 38 $kg.m^{-3}$) on average than cutover sites (Mean = 936 $kg.m^{-3}$, SD = 35 $kg.m^{-3}$) but the difference was not statistically significant (p-value = 0.3227).

Comparison Between Straight Trees and Defect Trees

The comparison between trees with and without defects is shown in Table 1.4. For the overall data, there was no significant difference in wood SG, wood MC and bark SG. The only significant difference was for bark MC where the bark MC in defect trees (Mean = 86%, SD = 25%) was lower than in non-defect trees (Mean = 95%, SD = 22%). There was significant difference between defect and non-defect trees for bark SG in cutover sites (p-value = 0.0248) where the bark SG in defect trees (Mean = 0.387, SD = 0.028) was higher than in non-defect trees (Mean = 0.371, SD = 0.025). There was also a significant difference between defect and non-defect trees for bark MC in old field sites (p-value = 0.0048) where the bark MC in defect trees (Mean = 99%, SD = 24%) was lower than in non-defect trees (Mean = 106%, SD = 21%). Generally, the p-

values for cutover sites (except for bark MC) were lower than in old-field sites, even though the sample size was smaller for cutover sites (N = 25) than old field (N = 31).

Table 1.4. Whole-tree specific gravity (SG) and moisture content (MC) values for different longleaf pine tissues in defect and non-defect trees. Significant differences due to defects are indicated by the p-values for each tissue.

Site Type	Tissue	Property	Non-Defects (N=135)				Defects (N=25)				*P*-value
			Mean	SD	Min	Max	Mean	SD	Min	Max	
Cutover	Wood	SG	0.502	0.039	0.424	0.612	0.520	0.049	0.444	0.620	0.1577
		MC (%)	105	17	70	140	99	17	69	130	0.1121
	Bark	SG	0.371	0.025	0.305	0.460	0.387	0.028	0.334	0.435	0.0248
		MC (%)	84	17	43	136	71	16	49	114	0.1448
	Tissue	Property	Non-Defects (N=129)				Defects (N=31)				*P*-value
			Mean	SD	Min	Max	Mean	SD	Min	Max	
Old field	Wood	SG	0.456	0.035	0.376	0.533	0.453	0.033	0.388	0.528	0.3088
		MC (%)	123	18	87	172	122	16	86	162	0.5092
	Bark	SG	0.346	0.036	0.254	0.412	0.350	0.043	0.262	0.519	0.7133
		MC (%)	106	21	67	160	99	24	50	173	0.0048
	Tissue	Property	Non-Defects (N=264)				Defects (N=56)				*P*-value
			Mean	SD	Min	Max	Mean	SD	Min	Max	
Overall	Wood	SG	0.479	0.044	0.376	0.612	0.482	0.052	0.388	0.620	0.8425
		MC (%)	113	19	70	172	112	20	69	162	0.5580
	Bark	SG	0.359	0.033	0.254	0.460	0.366	0.041	0.262	0.519	0.2549
		MC (%)	95	22	43	160	86	25	49	173	0.0029

Modeling Wood Specific Gravity

The parameters for the wood SG models are shown in Table 1.5 and the fit indices and error statistics are given in Table 1.6. Within a tree, the disk from the stump height had the greatest wood SG and it gradually decreased with increasing height. The rate of decrease in wood SG was slightly higher at relative heights from 0 to 0.10 and the rate of decrease slowed as relative height increased to the top of the tree bole. The base model for predicting wood SG as a function of relative height (Equation 3) explained 23% of the variation (fixed effects only) with RMSE 0.045 (Table 1.6). For the random effects, 33% of the variation was because of stand to stand variation, and 30% of the variation was due to variation among trees within stand. Incorporating the effect of age in the model (Equation 4) significantly improved the fit statistics over the base model (p-value = 0.0030) with the R^2 improving to 38% (RMSE = 0.040). Incorporating the effect of site type (Equation 5) further improved the model where the fixed effects explained 50% of the variation in the SG of the wood (RMSE = 0.036) and this model was significantly improved over the model with relative height and age (p-value <0.0001). Incorporating site type into the model reduced the random stand effect to account for 6% of the variation. Incorporating the effect of the tree defects on the wood SG (Equation 6) did not result in a significant parameter (p-value = 0.8420). Figure 1.2 shows the final model where wood SG is a function of relative height, age, and site type. The age shown was the mean age for the stands (age = 17.2 years).

Table 1.5. Parameter estimates for the wood and bark specific gravity (SG) models with their respective standard error (SE) values.

		Model					
Property	**Parameter**	**Base model (Eq. 3)**	**SE**	**+Age effect (Eq. 4)**	**SE**	**+Site type effect (Eq. 5)**	**SE**
Wood SG	β_0	0.432	0.008	0.335	0.029	0.365	0.018
	β_1	0.042	0.002	0.042	0.002	0.042	0.002
	β_2	0.145	0.019	0.145	0.019	0.145	0.019
	β_3	-	-	0.005	0.002	0.005	0.001
	β_4	-	-	-	-	-0.038	0.007
	Parameter	**Base model (Eq. 8)**	**SE**	**+Age effect (Eq. 9)**	**SE**	**+Site type effect (Eq. 10)**	**SE**
Bark SG	β_0	0.327	0.007	-	-	0.341	0.007
	β_1	0.018	0.001	-	-	0.018	0.001
	β_2	0.887	0.105	-	-	0.888	0.106
	β_3	-	-	-	-	-	-
	β_4	-	-	-	-	-0.029	0.009

Table 1.6. Fit indices and error statistics for the wood and bark specific gravity (SG) models. E represents the mean error. |E|% represents the mean absolute percent error.

			Fit Indices (R^2)			**Model Errors**		
Property	**Model**	**AIC**	**Fixed**	**Stand**	**Tree**	**E**	**RMSE**	**|E| %**
Wood SG	Base (Eq. 3)	-16977	0.23	0.56	0.86	0.0014	0.045	7.4508
	+Age (Eq. 4)	-16984	0.38	0.56	0.86	-0.0009	0.040	6.6612
	+Site type (Eq. 5)	-16999	0.50	0.56	0.86	-0.0003	0.036	6.0962
Bark SG	Base (Eq. 8)	-14359	0.29	0.50	0.66	0.0020	0.043	9.8560
	+Site type (Eq. 10)	-14364	0.37	0.50	0.66	0.0023	0.040	9.3714

Figure 1.2. Wood specific gravity fitted as a function of relative height, age, and site type for all the disks. The mean age is shown in the fitted line.

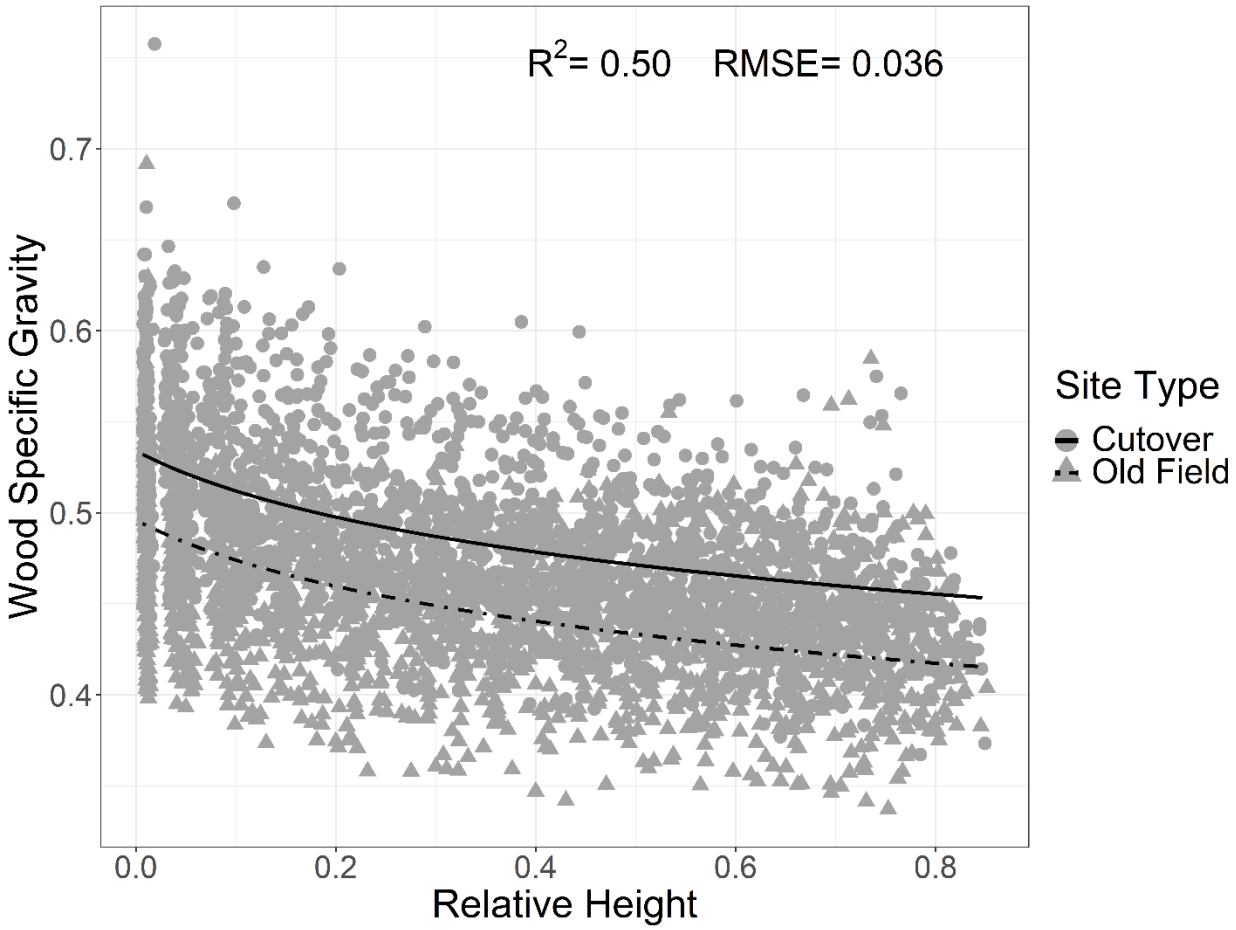

Modeling Wood Moisture Content

All the factors which affect wood SG (relative height, age, site type) directly or indirectly affect wood MC as wood SG and wood MC follow an inverse relationship. The model predicting wood MC as a function of wood SG (Equation 7) explained 86% of the variation (RMSE of 8.8%) in wood MC. The model parameters for equation 7 are β_0 and β_1 which are -194.602 and -1.169, respectively. The plot of wood MC as a function of wood SG is shown in Figure 1.3.

Figure 1.3. Wood moisture content fitted as a function of wood specific gravity for all the disks.

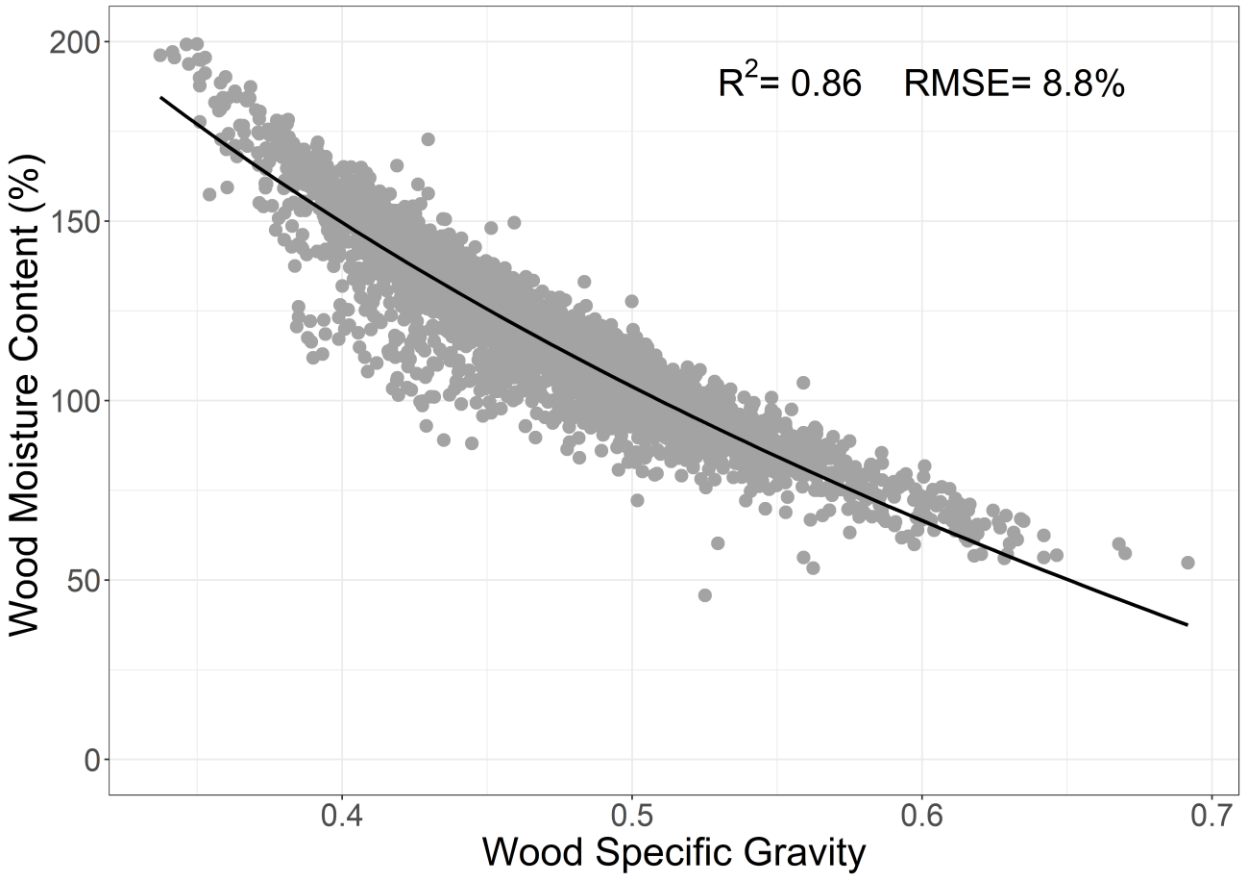

Modeling Bark Specific Gravity

The parameters for the bark SG models are shown in Table 1.5 and the fit indices and error statistics are given in Table 1.6. Bark SG decreased as a function of relative height, with a rapid decrease when relative height was less than 0.1. The base model for bark SG (Equation 8) explained 29% of the variation (fixed effects only) with RMSE of 0.043 (Table 1.6). Differences due to stands accounted for 21% of the variation and differences due to trees within stands accounted for 16% of the variation. Incorporating age into the model (Equation 9) was not

significant (p-value = 0.1079). Adding site type to the model (Equation 10) resulted in a significantly improved model (p-value = 0.0061). The model with added site type effect was able to explain 37% of the variation (RMSE = 0.040). Figure 1.4 shows the final model where bark SG is a function of relative height and site type.

Figure 1.4. Bark specific gravity fitted as a function of relative height and site type for all the disks.

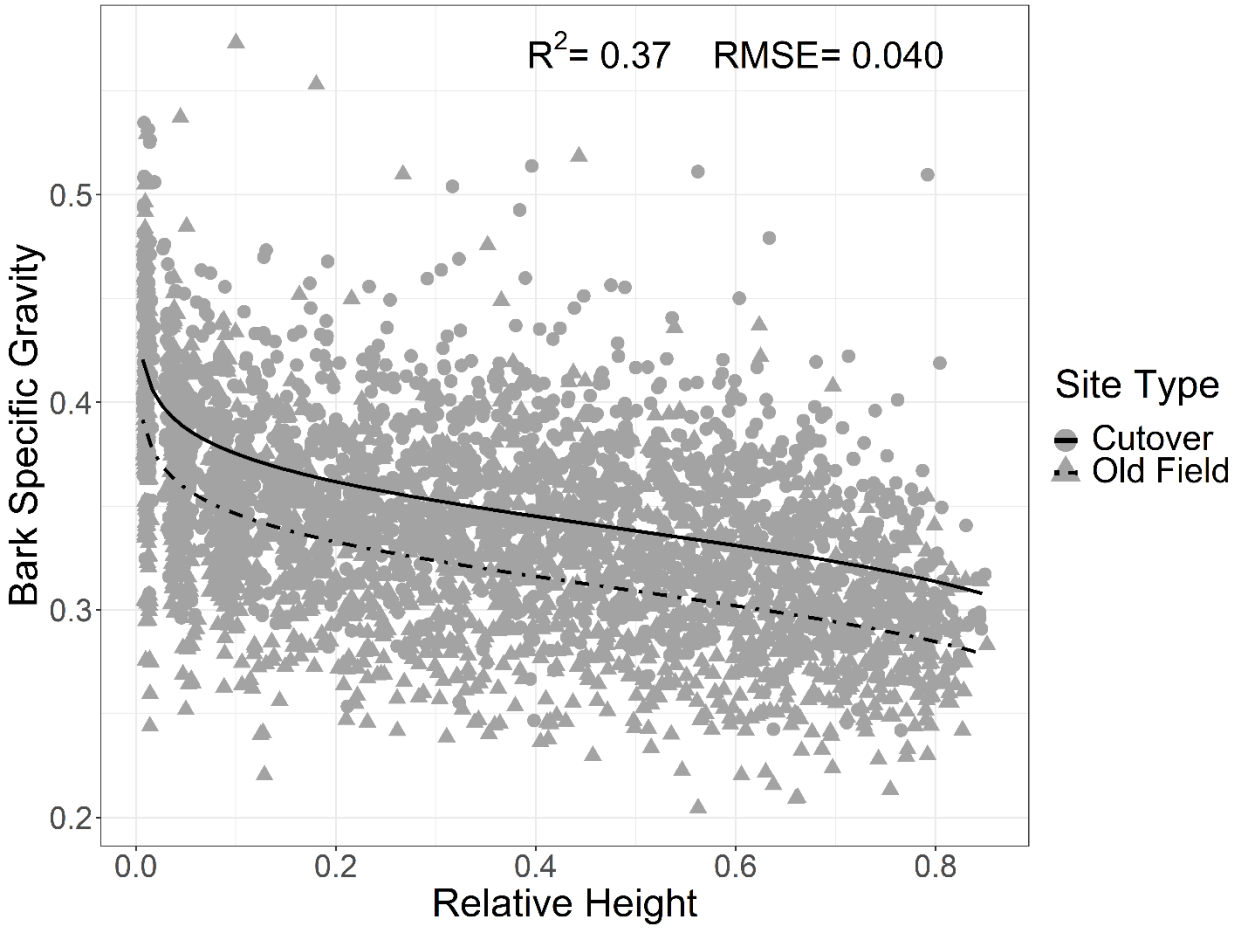

Modeling Bark Moisture Content

The model predicting bark MC as a function of bark SG (Equation 11) explained 69% of the variation (RMSE of 28.2%) in bark MC. The model parameters for Equation 11, β_0, β_1, and β_2 are 0.010, -0.086, and 0.243, respectively. Due to the factors that influenced the bark SG, bark MC varied as a function of relative height and site type. The plot of bark MC as a function of bark SG is shown in Figure 1.5.

Figure 1.5. Bark moisture content fitted as a function of bark specific gravity for all the disks.

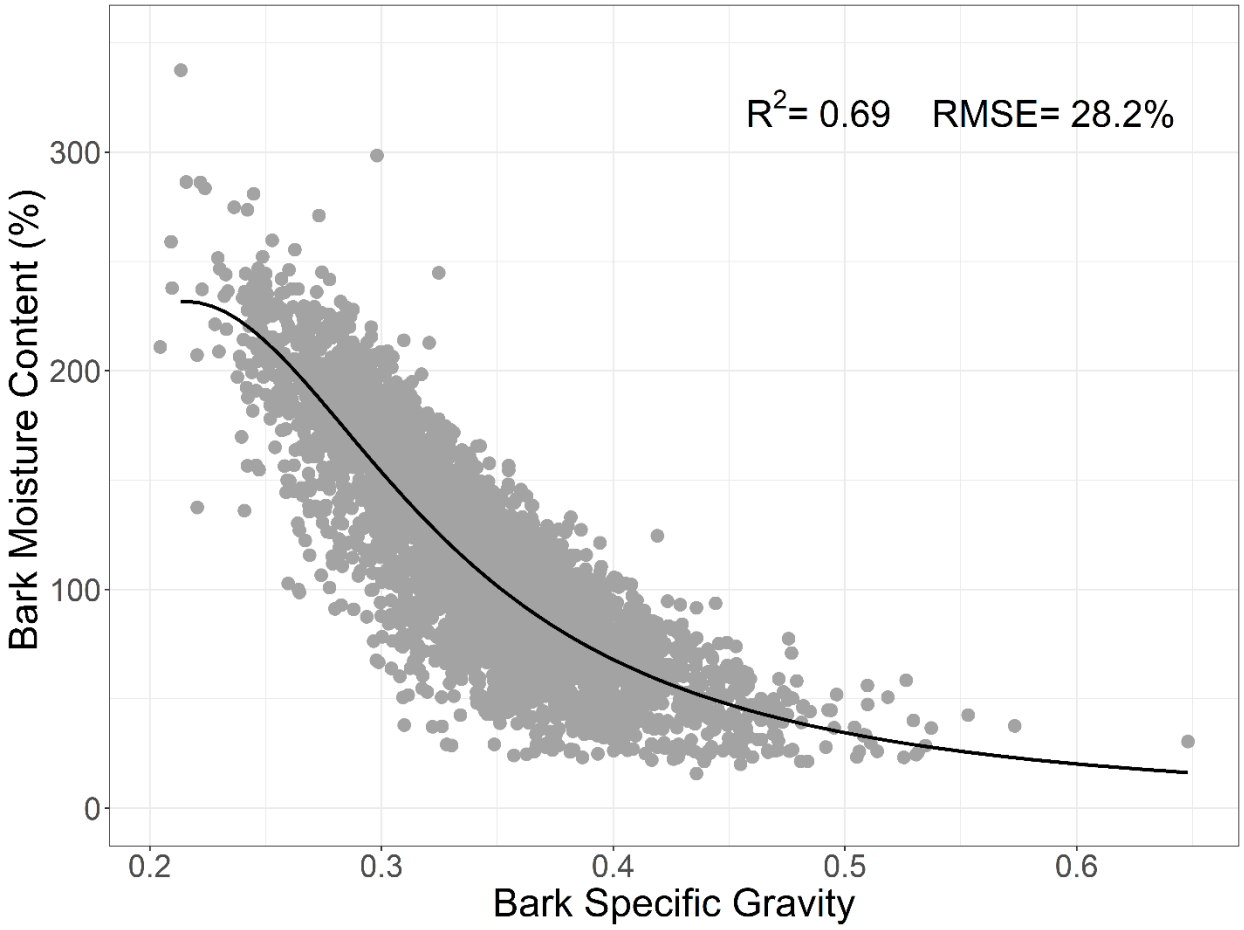

Diameter Inside Bark as a Function of Diameter Outside Bark

A simple linear model with no intercept (Equation 12) was used to fit DIB as a function of DOB, separately, for both cutover and old field sites as the difference between them was significant ($p < 0.0001$). For the cutover sites the β_1 parameter was 0.877 (R^2 of 0.98 and RMSE of 0.523 cm). For old field sites the β_1 parameter was 0.897 (R^2 of 0.99 and RMSE of 0.427 cm).

1.4 DISCUSSION

Wood

The mean whole-tree SG that we found (0.480) is similar to the value reported by Baldwin and Saucier (1983) for pulpwood size (DBH > 12.7 cm) unthinned longleaf pines planted on the Western Gulf cutover sites (0.500) which were planted at a density of 2470 trees ha^{-1} to 3700 trees ha^{-1}. Gibson et al. (1986) reported an average whole-tree wood SG of 0.482 in longleaf pines aged 26 years growing in dry sites in northern Louisiana with an initial planting density of 3000 trees ha^{-1}. All these wood SG values are less than the whole-tree SG (0.570) of 25-year-old longleaf pine trees planted at an initial density of 1075 trees ha^{-1} in cutover sites near Gulfport, Mississippi (Clark and Schmidtling 1989). From this study, the cutover stand 8 (which is also of age 25 years) had an average whole-tree wood SG of 0.547, similar to what Clark and Schmidtling (1989) report. Because ring SG increases with cambial age for southern pines, as stand age increases so too will whole-tree wood SG (Larson et al. 2001; Dahlen et al. 2018).

We found that cutover sites had higher whole-tree wood SG than old field sites even though the age was similar. For example, the 20 trees having the highest whole-tree wood SG were from

cutover sites. Clark and Schmidtling (1989) found that fertilization and site preparation increased the period of corewood (juvenile wood) production which reduced wood SG in longleaf pines planted in cutover sites. Love-Myers et al. (2010) found that fertilization lowered the overall wood SG in loblolly pine. An increase in juvenile wood proportion (having low SG) as a result of competition control of woody and herbaceous weeds was reported in loblolly pine by Antony et al. (2011). The old field sites likely had a lower wood SG because of the presence of residual nutrients from repeated fertilizer treatments and absence of competition from hardwoods in the initial growing years (Clabo et al. 2020). From a wood utilization perspective, the cutover sites had higher SG and lower MC wood and thus a forest products manufacturing facility would be buying more wood and less water compared to old field sites.

Compared to loblolly and slash pine, cutover sites had higher wood SG (0.504) than loblolly pine (0.480) and slash pine (0.475) both aged 26 years and growing on dry sites in northern Louisiana in the study by Gibson et al. (1986). Cutover sites had higher wood SG (0.504) than loblolly pine at age 25 (0.500) but lower wood SG than slash pine at age 25 (0.570) as reported by Clark and Schmidtling (1989). Samples used for this study were younger compared to those studied by Gibson et al. (1986) and Clark and Schmidtling (1989). In slightly older material than found here (age 21-24 years and initial planting density of approximately 1779 trees ha^{-1}), Eberhardt et al. (2017) found that loblolly pine (0.498) had lower SG than what we found for cutover sites (0.504), however old field material had lower SG (0.455) than loblolly pine, and slash pine had greater SG (0.523). Compared to the Wood Handbook (Kretschmann 2010) wood SG values for longleaf and slash pine (0.540), and loblolly and shortleaf pine (0.470), our values for wood SG in cutover sites (0.504) were higher than loblolly pine and shortleaf pine but lower than

longleaf pine or slash pine; however the age of the specimens is likely older for the Wood Handbook values.

Wood SG decreased with an increase in relative height. This trend in SG by height is common for other southern pines, including work by Eberhardt et al. (2017) on loblolly pine and slash pine, and Dahlen et al. (2018) on loblolly pine. Wood properties undergo rapid changes in the first 5 m from the base of the tree (Burdon et al. 2004), and for southern pines the trends with increasing height on SG is negative (Megraw 1985). Antony et al. (2010) reported that a stem of loblolly pine across different regions in the southeast US could be separated into three distinct segments, and their model forms confirmed that where the mean SG decreased rapidly from the base of the tree to a relative height of 0.1; it then decreased at a decreasing rate to a relative height of 0.3, and from then on, it decreased at a constant rate. The model used by Eberhardt et al. (2017) for explaining wood SG variation with respect to relative height in loblolly and slash pine showed that the wood SG decreased at an increasing rate to a relative height of 0.1; it then decreased at a constant rate to a relative height of 0.8 and decreased rapidly from there on. For planted longleaf pine, we found that though the wood SG decreased at a higher rate up to a relative height of 0.1 as compared to the upper regions along the tree height, the decrease in wood SG was not as sharp as in loblolly or slash pine.

The final wood SG model explained 50% of the variation with the variables relative height, age, and site type. The high tree to tree variation (30%) versus stand variation (6%) is typical for wood properties (Dahlen et al. 2018). The longleaf pine model has lower prediction statistics than what was found by Eberhardt et al. (2017) for loblolly pine ($R^2 = 0.77$) and slash pine ($R^2 = 0.60$). The Eberhardt et al. (2017) samples came from a designed growth and yield experiment and

sampled only three trees per stand which were close to the mean diameter class, whereas the longleaf pine sampled here were from operational stands where we sampled 20 trees per stand across the diameter distribution. Also the age range for our study was much broader (12 years - 25 years) whereas that for Eberhardt et al. (2017) was narrow (21 years - 24 years). At the ring level, wood SG increases non-linearly with cambial age (Jordan et al. 2008; Dahlen et al. 2018). At the disk level however, we found that age linearly increased wood SG; it is important to not extrapolate the results of this model to much older cambial ages.

Values of wood MC here are similar to those reported by Baldwin and Saucier (1983) in planted, unthinned longleaf pine trees grown on Western Gulf sites with a mean value of 110% with range of 76% - 142%. Koch (1972) reported species average wood MC for longleaf pine to be 100%. For comparison with loblolly and slash pine, whole-tree wood MC values were reported to be 106% (similar to cutover sites in our study – 104%) and 96%, respectively (Eberhardt et al. 2017). Whole-tree wood MC for old field sites in our study were higher (123%) than those reported for both loblolly and slash pines in Eberhardt et al. (2017) likely due to the lower SG. The higher wood MC in trees from old field sites would result in higher drying costs compared to cutover sites, as well as for a given green weight of wood cutover sites would yield more dry weight. Wood MC results correspond to wood SG results as it was expected for old field sites to have higher wood MC because they were found to have lower wood SG than cutover sites.

Defect vs Non-Defect Wood Differences

We did not find significant differences in wood SG or MC with regard to straight or defect containing trees. The defect trees sampled in this study consisted of forked trees, trees that had

ramicorn branches, and trees that had rust, in addition to the trees with excessive sweep. Occurrence of higher SG compression wood is expected for trees with excessive sweep but it is not always the same with wood from trees having other defects (Sharma et al. 2017). It is important to note that not every disk cut from a defect tree will have compression wood, and we did not separate disks with and without compression wood as this is difficult to determine on rough cut disks, except in cases where compression wood formation is severe. A study specifically focused on defect trees with a larger sample size could differentiate between the said defects and help to draw more informed conclusions.

Bark

The mean whole-tree bark SG that we found (0.360) is slightly lower than what was reported (0.389 with a range of 0.324 - 0.461) by Baldwin and Saucier (1983) for planted, unthinned longleaf pines. A slightly lower whole-tree bark SG (0.334) was reported by Gibson et al. (1986) for longleaf trees growing in drier sites. We found that longleaf pine has similar bark SG as slash pine (0.368), and higher bark SG than loblolly pine (0.311) (Eberhardt et al. 2017).

We found similar bark MC mean values (93% vs 90%) and ranges (43 – 173% vs 60% - 124%) as was reported by Baldwin and Saucier (1983) for planted, unthinned longleaf pine in the Western Gulf. For comparison, Eberhardt et al. (2017) found average bark MC for loblolly and slash to be 78% and 69%, respectively. Just like the relationship between wood MC and wood SG, bark MC also decreased as the bark SG increased (Figure 1.5). Bark MC is heavily influenced by the proportion of inner and outer bark with the inner bark thickness for longleaf pine remaining

somewhat constant but the outer bark thickness decreases along the length of the tree (Eberhardt 2013). As a result, the bark MC increases with increasing height within tree.

The effect of relative height on bark found here was very different from what Eberhardt et al. (2017) found for loblolly and slash pine. Here we found bark SG was highest at the stump, whereas Eberhardt et al. (2017) found little variation for slash pine, and loblolly pine had highest bark SG around mid-height, however the data was highly variable compared to the results found here. Here the final bark SG model explained 37% of the variation with relative height and site type as the fixed effects. There was more variability by stand (13% vs 6%) and less variability by tree (16% vs 30%) for bark than for wood, perhaps some of these differences could be due to specific silvicultural prescriptions done at the stand level, such as prescribed burning. Bark models from Eberhardt et al. (2017) for loblolly and slash pine had comparatively lower prediction statistics ($R^2 = 0.18$ for loblolly pine and $R^2 = 0.02$ for slash pine) which shows that bark is more predictable for planted longleaf pine as the models had higher prediction statistics ($R^2 = 0.37$) than those for planted loblolly or slash pine, however we are not sure why this is the case. With regards to the ratio between DOB and DIB, the amount of bark found here for cutover ($\beta_1 = 0.877$) and old field ($\beta_1 = 0.897$) was higher than what Dahlen et al. (2020a) report for loblolly pine ($\beta_1 = 0.932$). The relative accuracy of the DOB to DIB model ($R^2 = 0.98$ for cutover and 0.99 for old field) allows for precise predictions of DIB when measuring DOB, for example in the field.

Wood and Bark Green Weight

In the southern U.S., roundwood is sold on a green weight basis and thus accurate estimates of SG and MC of wood and bark help inform procurement decisions for forest products facilities

(Taras 1956; Antony et al. 2015; Eberhardt et al. 2017). Cutover sites had higher wood and bark SG and lower wood and bark MC as compared to old field sites, and thus utilizing trees from cutover sites would result in an industry paying less for water that they will need to remove during processing. The mean whole-tree wood green mass yield for this study (1016 kg m^{-3}) was slightly lower than what was reported for slash pine (1023 kg m^{-3}) and loblolly pine (1026 kg m^{-3}) which is likely due to the younger ages here (mean age 17.2 years) than those reported by Eberhardt et al. (2017) (21-24 years). For a combined given volume of wood and bark, the average wood and green bark mass yield from our study (942 kg m^{-3}) was still higher than those reported for loblolly (935 kg m^{-3}) and slash pine (930 kg m-3).

Fire Protection and Comparison to Loblolly and Slash Pine

Wang and Wangen (2011) from their study on 33-year-old longleaf pines subjected to biennial fire regimes concluded that frequent burning did not influence bark thickness or bark production. While not conclusive, our results appear to follow this conclusion. The double bark thickness values from this study are almost twice as that reported for loblolly and slash pine by Eberhardt et al. (2017), and the MC is also higher here (93%) than for loblolly pine (78%) or slash pine (69%). These differences might help explain the higher fire resistance in longleaf pine compared to other southern pines (Hardin et al. 2001). For a given bark MC, bark thickness is the most significant indicator of a tree's fire resistance (Bauer et al. 2010).

Utilization of Bark

Bark is an important raw material worldwide with the annual utilization amount exceeding 350 million m^3 (Pásztory et al. 2016). On a green weight basis, most conifer trees have 5% to 15% bark (Nosek et al. 2016). On a dry weight basis, energy content in bark is 2% higher as compared to that of wood (Kauter et al. 2003). In the southeastern United States nearly all forest product facilities burn bark for energy, however bark can be made into durable pellets (Lehtikangas 2001; Pásztory et al. 2016) and there is interest in utilizing bark in higher value products (Baker et al. 2012; Nosek et al. 2016; Pásztory et al. 2016; Eberhardt et al. 2017). On a dry weight basis, we found that planted longleaf pine had 17.8% dry mass of bark, which is higher than Eberhardt et al. (2017) found for both loblolly pine (12.5%) and slash pine (17%). Therefore, a bio-energy facility specifically focused on maximizing bark consumption would benefit more from planted longleaf pine bark as compared to loblolly or slash pine, and the bark from cutover sites would preferred over old field sites due to the lower moisture content which makes drying less expensive (Lehtikangas 2001).

1.5 CONCLUSION

Whole-tree SG and MC of wood and bark physical properties were measured for planted, unthinned longleaf pine trees grown in cutover and old field sites. Forest cutover sites had higher wood and bark SG than samples collected from old field sites. Wood and bark MC were higher for trees grown in old field sites because MC has an inverse relationship with SG for both wood and bark. Models were developed to describe the effects of relative height, stand age, and site type on wood and bark SG. Relative height and site type had a significant effect on both wood and bark

SG whereas age had significant effect on wood SG only. We did not find a significant difference between wood SG in trees with and without defects (forking, sweep, ramicorn branching, and rust). The results indicate that cutover sites produce higher quality wood that would be more suitable for lumber or Kraft pulp (for linerboard or dissolving pulp) than trees from old field sites. For a given green ton of wood and bark, cutover sites had a higher yield of wood and bark dry mass than old field sites. This work provided wood quality data for unthinned longleaf pine at the whole-disk level. Future work could be directed towards the use of X-ray densitometry to calculate ring by ring wood SG on older material to understand how wood SG changes with cambial age for longleaf pine from planted trees. Future research can also be done to better understand why the bark SG variability within tree was much more consistent for planted longleaf pine than planted loblolly or slash pine.

Acknowledgements

I would like to thank the NRCS for funding this project (project code: 68-4310-17-012). I am grateful to landowners Ben O'Conner, Chuck Fore, David Wells, Georgia Power, Heather Brassel, Joseph W. Jones Ecological Research Center at Ichauway, Lynda Beam, Lamar Zipperer, Larry Hardy, Mark Dixon, Pete Peebles, Pete Studstill, and Rayonier for allowing sample collection from their planted longleaf stands. I would also like to thank Bryan Simmons from the Wood Quality Consortium (WQC) and my fellow graduate students Thomas Harris and Mark Porter for their help with field work and sample collection.

REFERENCES

Antony, F., Schimleck, L.R., Daniels, R.F., Clark, A.III., and Hall, D.B. 2010. Modeling the longitudinal variation in wood specific gravity of planted loblolly pine (*Pinus taeda*) in the United States. Can. J. For. Res. **40**(12): 2439–2451. doi:10.1139/X10-187.

Antony, F., Schimleck, L.R., Daniels, R.F., Clark, A.III., Borders, B.E., Kane, M.B., and Burkhart, H.E. 2015. Whole-tree bark and wood properties of loblolly pine from intensively managed plantations. For. Sci. **61**(1): 55–66. doi:10.5849/forsci.12-030.

Antony, F., Schimleck, L.R., Jordan, L., Clark, A.III., and Daniels, R.F. 2011. Effect of early age woody and herbaceous competition control on wood properties of loblolly pine. For. Ecol. Manage. **262**(8): 1639–1647. doi:10.1016/j.foreco.2011.07.015.

ASTM International. 2017. D2395-17. Standard test methods for density and specific gravity (relative density) of wood and wood-based materials. ASTM International, West Conshohocken, PA. 13 p.

Baker, S.A., Greene, W.D., and Wilson, A. 2012. Fuels characteristics of woods-run whole tree southern pine chips. Biomass and Bioenergy **37**: 67–72. doi:10.1016/j.biombioe.2011.12.034.

Baldwin, V.C., and Saucier, J.R. 1983. Aboveground weight and volume of unthinned, planted longleaf pine on West Gulf forest sites. Res. Pap. SO-191. USDA Forest Service, Southern Forest Experiment Station, New Orleans, LA. 25 p.

Bauer, G., Speck, T., Blömer, J., Bertling, J., and Speck, O. 2010. Insulation capability of the bark of trees with different fire adaptation. J. Mater. Sci. **45**(21): 5950–5959. doi:10.1007/s10853-010-4680-4.

Becker, R.A., Wilks, A.R., Brownrigg, R., Minka, T.P., and Deckmyn, A. 2018. maps: Draw geographical maps. R package version 3.3.0. Available from URL https://CRAN.R-project.org/package=maps [accessed 3 April 2020.

Bivand, R., and Rundel, C. 2019. rgeos: Interface to geometry engine - open source ('GEOS'). R package version 0.5-2. Available from URL https://CRAN.R-project.org/package=rgeos [accessed 3 April 2020].

Brockway, D.G., and Lewis, C.E. 1997. Long-term effects of dormant-season prescribed fire on plant community diversity, structure and productivity in a longleaf pine wiregrass ecosystem. For. Ecol. Manage. **96**: 167–183.

Brockway, D.G., Outcalt, K.W., Tomczak, D.J., and Johnson, E.E. 2005. Restoration of longleaf pine ecosystems. Gen. Tech. Rep. SRS-83. USDA Forest Service, Southern Research Station, Asheville, NC. 35 p.

Burdon, R.D., Paul Kibblewhite, R., Walker, J.C.F., Megraw, R.A., Evans, R., and Cown, D.J. 2004. Juvenile versus mature wood: A new concept, orthogonal to corewood versus outerwood, with special reference to *Pinus radiata* and *P. taeda.* For. Sci. **50**(4): 399–415. doi:10.1139/x84-145.

Clabo, D.C., Dickens, E.D., and Moorhead, D.J. 2020. Old-Field Longleaf Pine (*Pinus palustris* Mill.) Long-Term Growth and Yield Response to Midrotation Fertilization. For. Sci. (Xx): 1–11. doi:10.1093/forsci/fxaa017.

Clark, A.III., Jordan, L., Schimleck, L., and Daniels, R.F. 2008. Effect of initial planting spacing on wood properties of unthinned loblolly pine at age 21. For. Prod. J. **58**(10): 78–83.

Clark, A.III., and Schmidtling, R.C. 1989. Effect of intensive culture on juvenile wood formation and wood properties of loblolly, slash, and longleaf pine. *In* Proceedings of the Fifth Biennial Southern Silvicultural Research Conference. Gen. Tech. Rep. S0-74. *Edited by* J.H. Miller. USDA Forest Service. Southern Forest Experiment Station., New Orleans, LA. 618 p.

Cram, M.M., Outcalt, K.W., and Zarnoch, S.J. 2010. Growth of longleaf and loblolly pine planted on South Carolina sandhill sites. South. J. Appl. For. **34**(2): 79–83. doi:10.1093/sjaf/34.2.79.

Dahlen, J., Auty, D., and Eberhardt, T.L. 2018. Models for predicting specific gravity and ring width for loblolly pine from intensively managed plantations, and implications for wood utilization. Forests **9**(6): 1–20. doi:10.3390/f9060292.

Dahlen, J., Nabavi, M., Auty, D., Schimleck, L., and Eberhardt, T.L. 2020a. Models for predicting the within-tree and regional variation of tracheid length and width for plantation loblolly pine. For. An Int. J. For. Res. 00. 1–14. doi:10.1093/forestry/cpaa018.

Dahlen, J., Schimleck, L., and Schilling, E. 2020b. Modeling and monitoring of wood moisture content using time-domain reflectometry. Forests **11**(4): 479. doi:10.3390/f11040479.

Dickens, D., Montes, C., and Moorhead, D. 2018. Stem quality summary for old-field planted, unthinned longleaf stands in Georgia. Outreach paper. Warnell School of Forestry and Natural Resources, University of Georgia, Athens, GA. Available from URL https://gatrees.org/wp-content/uploads/2020/02/Stem-Quality-Summary-for Old%E2%80%90field-Planted-Unthinned-Longleaf-Stands-in-Georgia.pdf [accessed 5 May 2020].

Dickens, D., and Moorhead, D.J. 2018. Longleaf pine-growth and yields and mean annual increments in planted stands from the Western Gulf region, South Carolina and Georgia long-term studies. Outreach paper. Warnell School of Forestry and Natural Resources, University of Georgia, Athens, GA. Available from URL https://bugwoodcloud.org/bugwood/productivity/pdfs/Longleaf_Growth_Yield_W_Gulf_SC_GA_Dec_2018_Final.pdf [accessed 5 May 2020]

Eberhardt, T.L. 2013. Longleaf pine inner bark and outer bark thicknesses: Measurement and relevance. South. J. Appl. For. **37**(3): 177–180. doi:10.5849/sjaf.12-023.

Eberhardt, T.L., Dahlen, J., and Schimleck, L. 2017. Species comparison of the physical properties of loblolly and slash pinewood and bark. Can. J. For. Res. **47**(11): 1495–1505. doi:10.1139/cjfr-2017-0091.

Eberhardt, T.L., So, C.L., and Leduc, D.J. 2018. Wood variability in mature longleaf pine: Differences related to cardinal direction for a softwood in a humid subtropical climate. Wood Fiber Sci. **50**(3): 1–14.

Frost, C.C. 1993. Four centuries of changing landscape patterns in the longleaf pine ecosystem. *In* Proceedings of the Tall Timbers Fire Ecology Conference, No. 18, The Longleaf Pine Ecosystem: ecology, restoration and management. *Edited by* S.M. Hermann. Tall Timbers Research Station, Tallahassee, FL. pp. 17–43.

Gibson, M.D., McMillin, C.W., and Shoulders, E. 1986. Moisture content and specific gravity of the four major southern pines under the same age and site conditions. Wood Fiber Sci. **18**(3): 428–435.

Hainds, M.J. 2004. Establishing longleaf pine seedlings on agricultural fields and pastures. *In* Proceedings of the 12th Biennial Southern Silvicultural Research Conference. Gen. Tech. Rep. SRS-71. *Edited by* K.F. Connor. USDA Forest Service, Southen Research Station, Asheville, NC. pp. 309–313.

Hardin, J.W., Leopold, D.J., and White, F.M. 2001. Harlow and Harrar's textbook of dendrology. *In* 9th edition. McGraw Hill. 544 p.

Haywood, J.D., Sayer, M.A.S., and Sung, S.J.S. 2015. Comparison of planted loblolly, longleaf, and slash pine development through 10 growing seasons in central Louisiana - an argument for longleaf pine. *In* Proceedings of the 17th Biennial Southern Silvicultural Research Conference. e-Gen. Tech. Rep. SRS-203. *Edited by* A.G. Holley, K.F. Connor, and J.D. Haywood. USDA Forest Service, Southen Research Station, Asheville, NC. pp. 383–390.

Hinchee, M.A.W., Mullinax, L.N., and Rottmann, W.H. 2010. Woody biomass and purpose-grown trees as feedstocks for renewable energy. *In* Plant Biotechnology for Sustainability Production of Energy and Co-products, Biotechnology in Agriculture and Forestry 66. *Edited by* P.N. Mascia, J. Scheffran, J.M. Widholm, and T. Nagata. Springer-Verlag, Berlin Heidelberg. pp. 155–208.

Johnson, R., and Gjerstad, D. 2006. Restoring the overstory of longleaf pine ecosystems. *In* The Longleaf Pine Ecosystem: Ecology, Silviculture, and Restoration. *Edited by* S. Jose, E.J. Jokela, and D.L. Miller. Springer, New York, NY. pp. 271–295.

Jordan, L., Clark, A.III., Schimleck, L.R., Hall, D.B., and Daniels, R.F. 2008. Regional variation in wood specific gravity of planted loblolly pine in the United States. Can. J. For. Res. **38**(4): 698–710. doi:10.1139/X07-158.

Katz, J. 2016. needs: attaches and install packages. R package version 0.0.3. Available from URL https://CRAN.R-project.org/package=needs [accessed 3 April 2020].

Kauter, D., Lewandowski, I., and Claupein, W. 2003. Quantity and quality of harvestable biomass from Populus short rotation coppice for solid fuel use—a review of the physiological basis and management influences. Biomass and Bioenergy **24**: 411–427.

Koch, P. 1972. Utilization of the southern pines. Agriculture handbook No.420. Vol. 1: The raw material. USDA Forest Service, Southern Forest Experiment Station, Washington D.C. 734 p.

Kretschmann, D.E. 2010. Mechanical Properties of Wood. *In* Wood handbook: wood as an engineering material. Centennial ed. Gen. Tech. Rep. FPL-GTR-190. *Edited by* R.J. Ross. USDA Forest Service, Forest Products Laboratory, Madison, WI.

Kush, J.S., Goelz, J.C.G., Williams, R.A., Carter, D.R., and Linehan, P.E. 2006. Longleaf pine growth and yield. *In* The Longleaf Pine Ecosystem: Ecology, Silviculture, and Restoration. *Edited by* S. Jose, E.J. Jokela, and D.L. Miller. Springer, New York, NY. pp. 251–267.

Landers, J.L., Van Lear, D.H., and Boyer, W.D. 1995. The longleaf pine forests of the southeast: requiem or renaissance? J. For. **93**(11): 38–44.

Larson, P.R., Kretschmann, D.E., Clark, A.III., and Isebrands, J.G. 2001. Formation and properties of juvenile wood in southern pines: A synopsis. Gen. Tech. Rep. FPL-GTR-

129. USDA Forest Service, Forest Products Laboratory, Madison, WI. doi:10.2737/FPL-GTR-129. 42 p.

Lehtikangas, P. 2001. Quality properties of pelletised sawdust, logging residues and bark. Biomass and Bioenergy **20**(5): 351–360. doi:10.1016/S0961-9534(00)00092-1.

Love-Myers, K.R., Clark, A.III., Schimleck, L.R., Dougherty, P.M., and Daniels, R.F. 2010. The effects of irrigation and fertilization on specific gravity of loblolly pine. For. Sci. **56**(5): 484–493. doi:10.1093/forestscience/56.5.484.

McIntyre, K.R., Guldin, J.M., Ettel, T., Ware, C., and Jones, K. 2018. Restoration on longleaf pine in the southern United States: a status report. *In* Proceedings of the 19th biennial southern silvicultural research conference. e-Gen. Tech. Rep. SRS-234. *Compiled by* J.E. Kirschman. USDA Forest Service, Southen Research Station, Asheville, NC. p. 444.

McKeand, S., Mullin, T., Byram, T., and White, T. 2003. Deployment of genetically improved loblolly and slash pines in the south. J. For. **101(3)**(3): 32. doi:10.1093/jof.101.3.32.

Megraw, R.A. 1985. Wood quality factors in loblolly pine: The influence of tree age, position in tree, and cultural practice on wood specific gravity, fiber length, and fibril angle. TAPPI Press, Peachtree Corners, GA, USA. 88 p.

Moore, J.R., and Cown, D.J. 2017. Corewood (juvenile wood) and its impact on wood utilisation. Curr. For. Reports **3**(2): 107–118. doi:10.1007/s40725-017-0055-2.

Mora, C.R., Allen, H.L., Daniels, R.F., and Clark, A.III. 2007. Modeling corewood-outerwood transition in loblolly pine using wood specific gravity. Can. J. For. Res. **37**(6): 999–1011. doi:10.1139/X06-250.

Nicholls, J.W.P. 1982. Wind action, leaning trees and compression wood in *Pinus radiata* D. Don. Aust. For. Res. **12**(2): 75—91.

Nosek, R., Holubcik, M., and Jandacka, J. 2016. The impact of bark content of wood biomass on biofuel properties. BioResources **11**(1): 44–53. doi:10.15376/biores.11.1.44-53.

Nyström, J., and Kline, D.E. 2000. Automatic classification of compression wood in green southern yellow pine. Wood Fiber Sci. **32(**3): 301–310.

Oswalt, C.M., Cooper, J.A., Brockway, D.G., Brooks, H.W., Walker, J.L., Connor, K.F., Oswalt, S.N., and Conner, R.C. 2012. History and current condition of longleaf pine in the southern United States. Gen. Tech. Rep. SRS-166. USDA Forest Service, Southern Research Station, Asheville, NC. 60 p.

Outcalt, K.W. 1993. Southern pines performance on sandhills sites in Georgia and South Carolina. South. J. Appl. For. **17**(2): 100–102. doi:10.1093/sjaf/17.2.100.

Pásztory, Z., Mohácsiné, I.R., Gorbacheva, G., and Börcsök, Z. 2016. The utilization of tree bark. BioResources **11**(3): 7859–7888. doi:10.15376/biores.11.3.Pasztory.

Pebesma, E. 2018. Simple features for R: standardized support for spatial vector data. R J. **10**(1): 439-446. Available from URL https://doi.org/10.32614/RJ-2018-009 [accessed 3 April 2020.

Pinheiro, J., Bates, D., DebRoy, S., Sarkar, D., and R Core Team. 2018. nlme: linear and nonlinear mixed effects models. R package version 3.1-137. Available from URL https://cran.r-project.org/web/packages/nlme/ [accessed 3 April 2020].

Pont, D., Brownlie, R.K., and Grace, J.C. 2007. Disc image-processing software for three-dimensional mapping of stem ring width and compression wood. New Zeal. J. For. Sci. **37**(2): 169–185.

R Core Team. 2020. R: a language and environment for statistical computing. R Foundation for Statistical Computing, Vienna, Austria. Available from URL https://www.R-project.org/ [accessed 3 April 2020].

Ratkowsky, D.A. 1990. Handbook of Nonlinear Regression Models. Marcel Dekker, New York. 241 p.

RStudio. 2020. RStudio: integrated development for R. RStudio, Inc., Boston, MA. Available from URL http://www.rstudio.com/ [accessed 3 April 2020].

Schimleck, L., Antony, F., Dahlen, J., and Moore, J. 2018. Wood and fiber quality of plantation-grown conifers: A summary of research with an emphasis on loblolly and Radiata pine. Forests **9**(6). doi:10.3390/f9060298.

Schimleck, L., Dahlen, J., Apiolaza, L.A., Downes, G., Emms, G., Evans, R., Moore, J., Pâques, L., Van den Bulcke, J., and Wang, X. 2019. Non-destructive evaluation techniques and what they tell us about wood property variation. Forests **10**(9). doi:10.3390/f10090728.

Schultz, R. 1999. Loblolly-the pine for the twenty-first century. New For. **17**: 71–88.

Scurfield, G. 1973. Reaction wood : Its structure and function. Science. **179**(4074): 647–655.

Sharma, M., Walker, J.C.F., and Chauhan, S.S. 2017. Screening corewood of pine for wood properties. *In* Wood is Good: Current Trends and Future Prospects in Wood Utilization. *Edited by* K.K. Pandey, V. Ramakantha, S.S. Chauhan, and A.N.A. Kumar. Singapore. pp. 19–27. doi:10.1007/978-981-10-3115-1_2.

South, A. 2017. rnaturalearth: world map data from Natural Earth. R package version 0.1.0. Available from URL https://CRAN.R-project.org/package=rnaturalearth [accessed 3 April 2020].

South, A. 2017. rnaturalearthdata: world vector map data from Natural Earth used in 'rnaturalearth'. R package version 0.1.0. https://CRAN.R-project.org/package=rnaturalearthdata [accessed 3 April 2020].

South, D.B. 2006. Planting longleaf pine at wide spacings. Nativ. Plants J. **7**(1): 79–88. doi:10.2979/npj.2006.7.1.79.

Timell, T.E. 1986. Compression wood in gymnosperms. Springer-Verlag, Berlin ; New York. 2150 p.

VanLear, D.H., Carroll, W.D., Kapeluck, P.R., and Johnson, R. 2005. History and restoration of the longleaf pine-grassland ecosystem: Implications for species at risk. For. Ecol. Manage. **211**(1–2): 150–165. doi:10.1016/j.foreco.2005.02.014.

Wang, G.G., and Wangen, S.R. 2011. Does frequent burning affect longleaf pine (*Pinus palustris*) bark thickness? Can. J. For. Res. **41**(7): 1562–1565. doi:10.1139/x11-074.

Wear, D., and Greis, J. 2012. The southern forest futures project: summary report. Gen. Tech. Rep. SRS-168. USDA Forest Service, Southen Research Station, Asheville, NC. doi:10.1017/CBO9781107415324.004. 54 p.

Wickham, H. 2011. The split-apply-combine strategy for data analysis. J. Stat. Softw. **40**(1):1-29. Available from URL http://www.jstatsoft.org/v40/i01/ [accessed 3 April 2020].

Wickham, H. 2016. ggplot2: elegant graphics for data analysis. Springer-Verlag, New York, NY. 260 p.

CHAPTER 2

A COMPUTER VISION APPROACH TO ASSESS WOOD VARIABILITY FROM WHOLE-DISK IMAGES OF LONGLEAF PINE[2]

[2] Raut, S and Dahlen, J. To be submitted to [Computers and Electronics in Agriculture]

ABSTRACT

Nondestructive evaluation (NDE) has become an increasingly important method for measuring wood properties to determine if they meet the requirements for specific end uses. Image analysis as an NDE tool is extensively used in forestry and forest products industries to rapidly and efficiently detect variability in wood. An objective of this study was to determine if image analysis was a suitable alternative to reference methods of measuring wood and bark volumes through water displacement. A total of 1120 cross-sectional disks extracted from multiple height levels of 104 straight and defect longleaf pine trees grown in 16 different stands across Georgia were used here. Disks were machined on one side using a computer numeric controlled router to prepare a surface for imaging. Three images; first under white light, second under blue light, and third under blue light with a green filter, respectively, were taken for each disk to allow for isolation of wood and bark components. Wood and bark volumes estimated from images were in close agreement with those measured using water displacement with the images slightly overpredicting the volume estimates. Linear models fitted as measured volumes versus image volumes for wood and bark had R^2 values of >0.99 and 0.96, and RMSE of 26.5 cm^3 and 3.9 cm^3 respectively. Outside bark and inside bark diameters estimated from images were also in close agreement with measurements made using a diameter tape, the inside bark estimates from images being almost the same as the measurements using a diameter tape. Linear models fitted as measured diameters versus image estimated diameters had R^2 values of >0.99 for both, and RMSE of 0.32 cm and 0.09 cm for outside and inside bark diameters, respectively. Four inside bark radii for each disk were used to calculate out of round (%) with the threshold set at 40% to separate ‘round’ and ‘not round’ disks. Not round and round disks were segmented for compression wood occurrence, with algorithms able to

identify severe compression wood but not mild compression wood. The majority of the ‘not round’ disks were from defect trees, and the disks that were more out of round and had higher quantities of severe compression wood came from trees that had excessive sweep. An additional advantage to imaging is the digital record of the disk which can be used for a number of other applications.

Keywords: bark, diameter inside bark, diameter outside bark, nondestructive evaluation, southern pine, wood and bark volume, wood imaging, wood and fiber quality

2.1 INTRODUCTION

Nondestructive evaluation of wood is increasingly being used in forestry and forest products research, operations and manufacturing (Ross and Pellerin 1994; Ross 2015; Schimleck et al. 2019). Imaging is one type of nondestructive evaluation tool and it has seen extensive use in a number of forestry and forest products applications (Evans 1994; Bucur 2003a, 2003b; Decellee et al. 2019; Wright et al. 2019). For example, a major industrial application of imaging is in lumber manufacturing facilities (Sauter et al. 2019). Sawmills accurately measure the shape and volume of logs using high-resolution laser scanners after the bark is peeled (Thomas and Bennett 2014). Rapid quantification of knots is now routinely achieved using the 'tracheid effect' where a camera detects the returned orientation of a laser beam projected onto wood, deviations from the longitudinal direction in the returned beam indicate localized slope of grain or knots which significantly lower the mechanical properties of wood (Nyström 2003; Roblot et al. 2010; Habite et al. 2019). Knots within logs and other defects have also been assessed using X-ray computed tomography images (Brüchert et al. 2019).

Outside of industrial applications, imaging has been employed in a number of wood and fiber quality research areas. The SilviScan suite of instruments collects monochrome images captured using near-infrared light to rapidly measure the dimensions of tracheids on solid polished samples (Evans 1994; Schimleck et al. 2019). The SilviScan system also measures microfibril angle variability radially using X-ray diffraction techniques (Evans et al. 1999). Light transmission in samples has been used to measure spiral grain (Riddell et al. 2012). Imaging in combination with machine learning techniques has been used to identify wood species (Yadav et al. 2017).

Clearly imaging is a versatile nondestructive evaluation tool, one exciting possibility on the use of imaging is in wood and fiber property studies to better capture variability on whole disks.

Wood properties including specific gravity (SG) (wood density divided by the density of water) vary significantly, with variation within annual rings, radially from pith to the bark via changes that occur as cambial age increases, and from the stump to the tip (Megraw 1985; Burdon et al. 2004; Dahlen et al. 2018). Some of the variation can be differentiated visually, for example differences in the physical appearance are often clearly evident from the stump to the tip. Within an individual annual ring, if compression wood is formed it is generally darker in color than normal earlywood but lighter than normal latewood (Timell 1986). Stem diameter decreases with increasing height from the stump (tree bottom) to the tip (tree top), and the rate at which the change in diameter occurs is termed as taper (Burkhart and Tomé 2012). While total bark thickness decreases with increasing stem height corresponding to the changes in overall diameter, the inner bark thickness remains relatively constant (Eberhardt 2013). Thus thickness changes in bark are due to thickening of the outer bark, with the stump height having the thickest outer bark as well as a more complex shape with numerous fissures (Eberhardt 2015). Typical field measurement of outside bark diameter is done using a diameter tape, with the inside bark diameter estimated using a ruler in two locations following tree felling. Inside bark diameter is more accurately measured as the difference between outside and inside bark diameter following careful peeling of the bark from the wood (Eberhardt et al. 2017). Field diameter measurements are typically assumed circular with evaluation of the tree shape done qualitatively.

In southern pines including longleaf pine, wood SG increases with cambial age, and for a given ring decreases with increasing height within tree (Larson et al. 2001; Dahlen et al. 2018). To

calculate the SG of wood of whole disks or bark SG and because wood and bark is non-uniform in shape, green volume is measured using water displacement (ASTM International 2017). Here, imaging presents an opportunity to replicate the volume measurements needed for SG calculation, as well as other measurements including diameter. A challenge with obtaining high quality images from wood disks is the initial rough-cut surface is poor quality (Figure 2.1). Provided that surface quality can be improved, the use of imaging is promising not only for the replication or replacement of measurements, but also because imaging presents opportunities to further extract information from disks. These additional measurements include assessments of disk shape and out of roundness, and compression wood quantity, among others. Another important advantage of imaging is being able to store a digital record of the samples, since due to space considerations it is not typically feasible to store presents well beyond the conclusion of a study. Opportunities to match the image with reconstructed models, to show within tree variation with images, or even determining outliers in data due to input errors, etc. are possible with images. Hence, the objective of this study was to compare wood and bark volume information and inside and outside bark diameters estimated using images of longleaf pine (*Pinus palustris)* disks with the reference measurements. We hypothesize that imaging can be used as reference measurements with high accuracy. Additional objectives are to use the images to measure disk shape and estimate the quantity of compression wood. We collected images on green disks above the fiber saturation point without any drying to save measurement time and reduce cracking that occurs during drying of disks.

Figure 2.1: Image showing typical surface quality of a chainsaw cut wood disk (left). The image on the right shows the same disk after surface preparation.

2.2 MATERIALS AND METHODS

Tree Selection and Disk Extraction

Samples used for this study were collected from 16 stands of planted, unthinned longleaf pine trees throughout South Georgia. Stands sampled were from old agricultural fields or cutover sites, with eight stands sampled per type. For each stand, an inventory was conducted using three $1/25^{th}$ hectare plots to obtain the diameter distribution of the trees. Trees were classified into straight trees (no visible defects), or as defect trees. Defect trees contained a visible defect such as a fork, excessive sweep, ramicorn branching, or fusiform rust, with the defect type recorded. From each stand, 20 trees were felled, with up to 6 defect trees sampled based on the frequency of defect trees within each stand. A subsample representing all of the defect trees sampled from each stand, and 3 randomly selected non-defect trees from each stand representing a suppressed (small), co-dominant (medium), and dominant (large) tree were selected and used for the study.

Trees were felled using a chainsaw, branches delimbed, and cross-sectional disks (approximate thickness 5 cm) were extracted using a chainsaw. Disks were collected at fixed intervals; 0.15 m (stump height), 0.6 m, 1.37 m (breast height), 2.44m, and from there at every 1.22 m interval along the tree bole up to the point where the outside bark diameter was 7.6 cm. When the fixed disk height overlapped branch whorls, the height was adjusted and the exact height recorded. From the forked trees, disks were extracted from the same fixed height intervals up to the crotch base. A disk was collected at the crotch base, from the base of each of the forks, and then from the height of the forks where the outside bark diameter was 7.6 cm. For each disk the relative height was calculated (disk height within the tree divided by the total height) which ranges from 0 (stump) to 1 (tip). A total of 104 trees and 1120 cross sectional disks were used here, with 56 defect trees (a total of 575 cross-sectional disks) and 48 straight trees (a total of 545 cross-sectional disks) (Table 2.1). The disks were labelled, placed in plastic bags, sealed, and transported from the field to a freezer in the Wood and Fiber Quality lab at the University of Georgia where they were kept frozen until further processing.

Table 2.1. Summary of the diameter outside bark (DOB) and diameter inside bark (DIB) for the cross-sectional disks used in this study.

		Non-Defects					**Defects**				
Site Type	**Property**	**N**	**Mean**	**SD**	**Min**	**Max**	**N**	**Mean**	**SD**	**Min**	**Max**
Cutover (N = 519)	DOB (cm)	268	13.8	5.0	6.3	30.9	251	13.2	4.5	6.3	23.6
	DIB (cm)		12.2	4.5	5.6	28.2		11.6	3.9	5.6	20.8
Old field (N=601)	DOB (cm)	277	15.5	5.8	6.6	32.5	324	14.4	5.0	6.3	27.7
	DIB (cm)		14.0	5.2	5.8	29.7		12.9	4.5	5.3	23.9
Overall (N = 1120)	DOB (cm)	545	14.6	5.5	6.3	32.5	575	13.9	4.8	6.3	27.7
	DIB (cm)		13.1	4.9	5.6	29.7		12.3	4.3	5.3	23.9

Disk Surfacing and Imaging

The disks were removed from the freezer and thawed for 48 hours after which the disks were removed from their plastic bags. A 3-axis computer numerical controlled (CNC) router (Fine Line Automation, Lebanon, PA, USA) built from a kit was used for machining the surface of the disks (Figure 2.2).

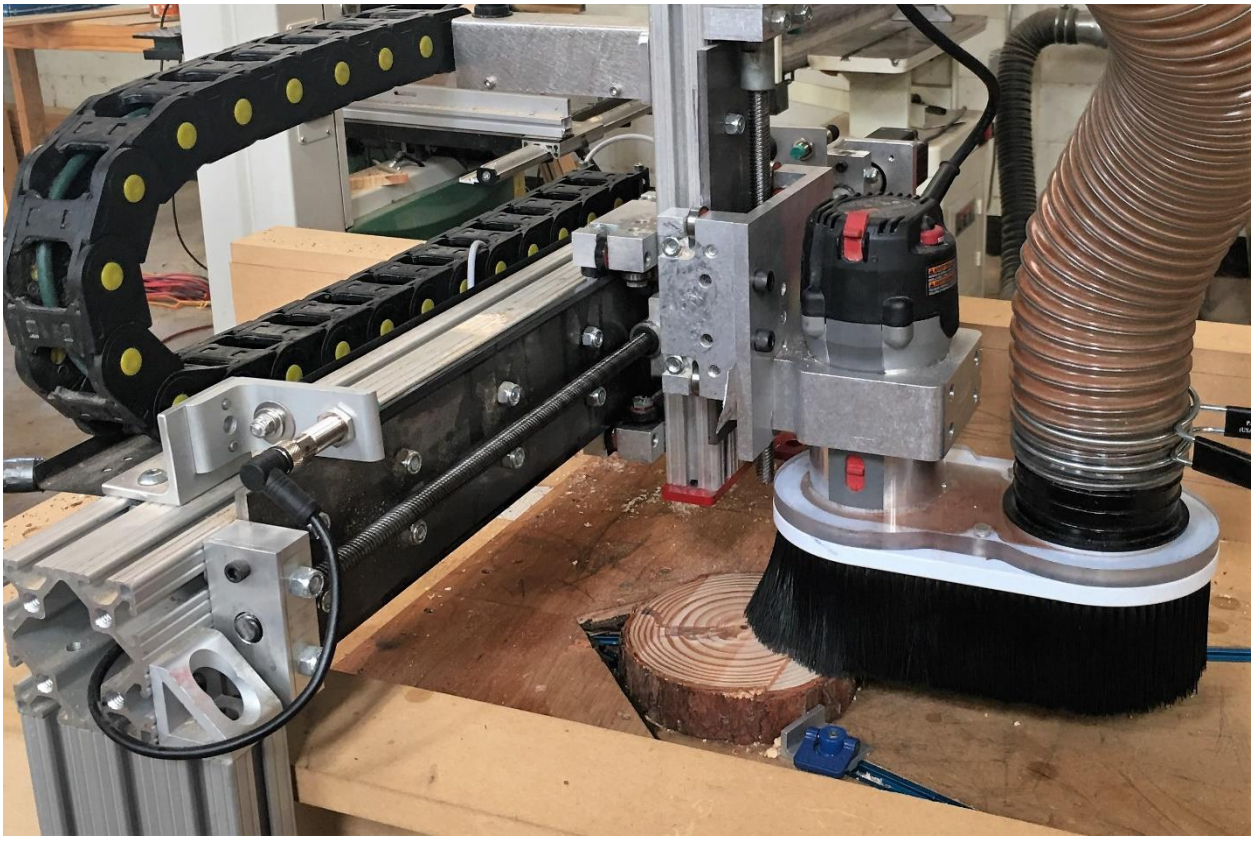

Figure 2.2. The 3-axis computer numerical controlled (CNC) router preparing a cross-sectional disk surface for imaging.

The CNC router was controlled using an Arduino (Arduino AG, Somerville, MA, USA) with stepper motors used for the linear motion. Since the disks were cut in the field using a

chainsaw, the disk height varies. We used an ultrasonic distance sensor (Micro Detectors UK6, Modena Italy) mounted on the y-axis on the CNC router to measure the height of the disk and the size of the disk. We then adjusted the router cut depth based on the disk height, and adjusted the router cutting path based on the disk size. The cutting bit used was an Amana Tool RC-2257 surface planer (Newton, IA, USA). The router cut 2 passes on each disk, the first pass alternated the cut direction from left to right using the y-axis, where the router took off 6.4 mm off the height of the disk (z-axis) in 28 mm passes (x-axis). The second pass skimmed the disk with 0.3 mm cut depth (z-axis) in 60.5 mm passes (x-axis). The second pass was done cutting from left to right, and after each pass the router returned to the left position of the y-axis before moving up on the x-axis. The second pass made the surface of the disk more even which improved imaging.

Following surface preparation, images of the disks were taken using a custom-built setup with a white background and controlled using an Arduino which interfaced to a computer running Python (Python Software Foundation, https://www.python.org/). Communication between the Arduino and Python was done using serial commands. The camera used was an Allied Vision Manta G-1236 with a 12.4-megapixel sensor (Stradtroda, Germany) and a 12 mm lens (Computar, Cary NC, USA). The camera control was done using the Pymba library (https://github.com/morefigs/pymba). Prior to imaging, the disk thickness was read by an ultrasonic sensor (Micro Detectors UK6, Modena, Italy). A linear translation stage with a stepper motor moved the top surface of the disk to 600 mm distance from the camera based on the disk thickness reading from the ultrasonic sensor. Thus, each disk was imaged with a fixed focal length from the camera to ensure accurate calculation of diameter and area measurements.

We found that different steps in image processing were best achieved when the disks were lit using different sources. As such, lighting for the disks was done using two LED light sources mounted in tracks; white light with 4,000K color temperature LEDs, and blue light (475 nm) LEDs (Super Bright LEDs Inc, St. Louis, MO, USA). One challenge in working with images that contain both wood and bark was isolating the bark from the wood. During initial tests that were focused on using fluorescence imaging techniques with the blue LEDs and a 50 mm diameter green longpass filter (>525 nm) (Edmund Optics, Barrington, NJ, USA) to detect compression wood (Thomas 2014), we observed that that the fluorescence image had clear separation between the bark and the wood. A total of three red-green-blue (RGB) images were taken for each machined disk. The first image was taken using white light with 12,500 µs exposure time (herein referred to as the white image). The second image was taken using blue light with 80,000 µs exposure time (herein referred to as the blue image). The third image was taken under blue light with 500,000 µs exposure time with the longpass filter in front of the lens (herein referred to as the filter image). For the filter image, the longpass filter was moved in front of the lens using a stepper motor, and following image collection the filter was rotated away from the lens. The three images for one disk are shown in Figure 2.3, note that the paint used to mark the location on the tree to cut disks fluorescence's and appears bright orange in the filter image (note this was not intended and only discovered after field sampling). Images were saved with each color channel having 8-bit depth, so pixel values ranged from 0 to 255 for each channel.

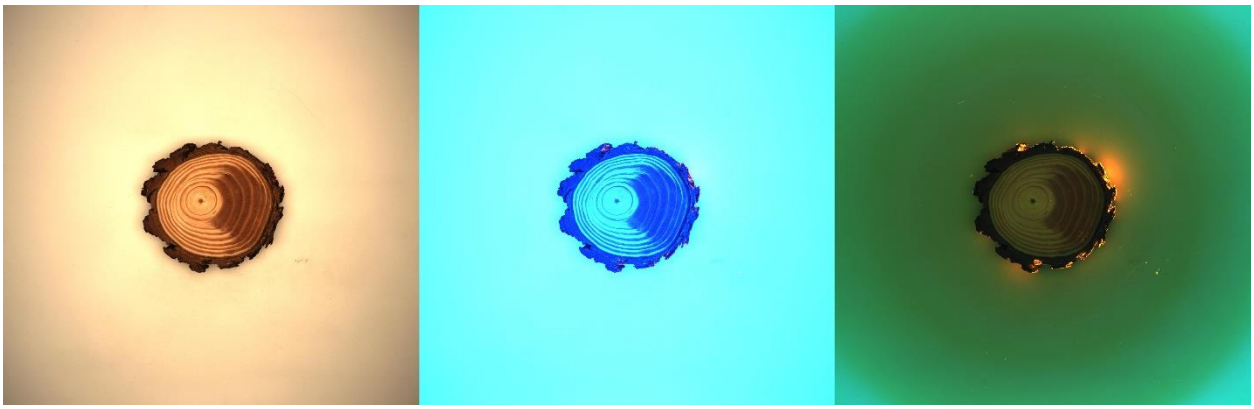

Figure 2.3. A set of three images taken for a machined disk diameter outside bark (DOB) of 17.3 cm. Left: white image; middle: blue image; right: filter image.

Disk Measurements

Following imaging, the outside bark diameter was measured with a diameter tape and the disks were weighed on a digital scale. We then peeled off the bark, measured the inside bark diameters, and weighed the disk again. The difference in weight of the disk with and without bark gave the total bark weight. The largest chunk of bark from each disk was used for volume measurement where it was labelled and submerged in water for 48-72 hours. The peeled disks were also submerged in water for the same amount of time. Following submerging the samples, the bark pieces and the peeled disks were measured for their green volume using water displacement (ASTM International 2017). The green volume of the bark piece was then extrapolated to the total bark green volume using the total bark weight for each disk.

Image Processing

Image processing was done in Python version 3.7 (Python Software Foundation, https://www.python.org/) on the Spyder interface using the libraries OpenCV (Bradski 2000),

NumPy (Oliphant 2006), and pandas (McKinney 2010). The camera was calibrated using various objects of known sizes and the lens was checked for distortion using OpenCV (Bradski 2000).

Background Isolation

The first step in image processing was to isolate the background from the wood and the bark. Here we used the green channel of the blue image because the background was uniformly bright (pixel value = 255), whereas the wood and bark were darker (Figure 2.4). A mask of the background was created by thresholding the image with any pixel less than 255 being converted to 0 (wood and bark), and any pixel equal to 255 as white (background) (Figure 2.4). The mask from each disk was then applied to the white, blue, and filter images (Figure 2.5).

Figure 2.4. Image showing the green channel of the blue image (left) and an image of the whole-disk mask (right).

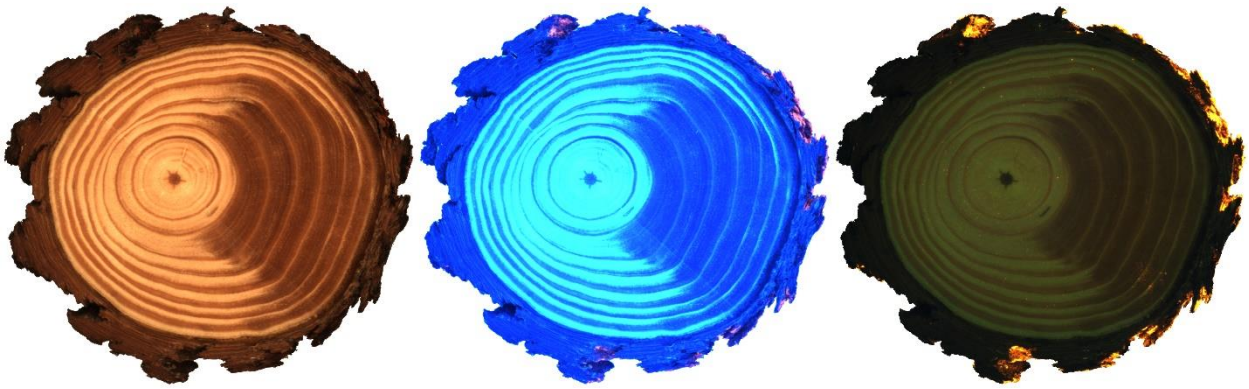

Figure 2.5. White (left), blue (middle), and filter (right) images after the whole-disk mask was applied on the original images (note that image is cropped).

Wood and Bark Isolation

After isolating the background, we manually determined the location of the pith by loading each image into Python, clicking on the centre of the pith using a mouse, and saving the pith coordinates. The red channel of the filter image was used to isolate the bark from the wood because the inner bark near the wood was uniformly dark and thus enabled clear separation from the wood and the bark. The one area where the bark was similar to the wood was at the pith, which is made up of ground tissue, rather than the rest of the wood made up of secondary xylem tissue (Beck 2010). To isolate the pith from the bark, we applied a white mask at the pith using the coordinates of the pith (Figure 2.6, image on the left). An initial mask of the bark was created by thresholding the image with any pixel less than 30 being converted to 255 (white) and the rest of the pixels converted to 0 (black). We then applied the bark mask on the whole-disk image to remove the bark, however some regions on the outside of the bark was bright due to the orange paint that fluorescence's (Figure 2.3, image on the right). To correct for this, we retained the largest contour (Arbeláez et al. 2011; Papari and Petkov 2011) of the image, which was the wood. The largest

contour was converted to a mask of the wood by itself. A corrected bark mask (Figure 2.6, middle image) was then created using the whole-disk mask and the wood mask. The wood mask was applied to each disk to isolate the bark from the wood (Figure 2.6, right image).

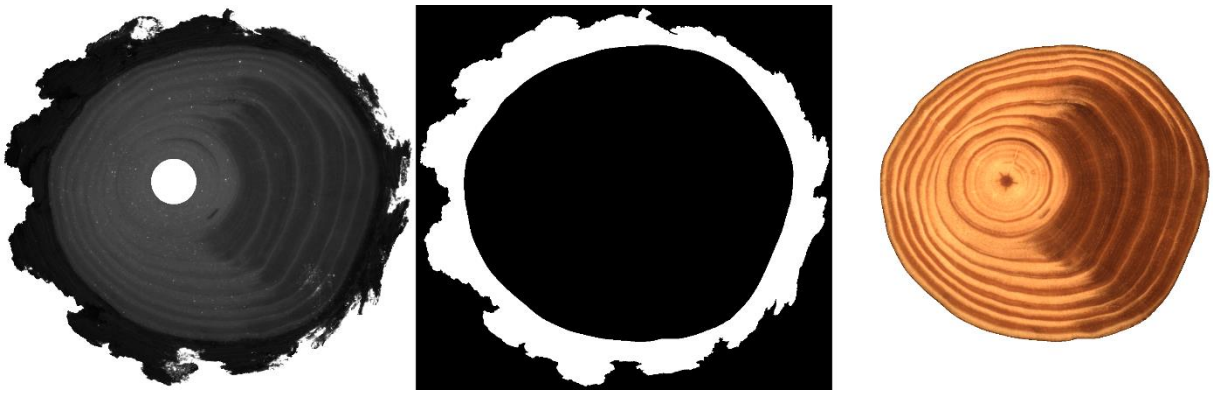

Figure 2.6. The left image shows the red channel of the filter image with a white mask applied to the pith and the wood appearing lighter than the dark inner bark. The middle image shows the bark mask made using the whole-disk mask and the wood mask found after finding the largest contour. The right image shows the isolated wood after applying the mask.

Wood and Bark Area

The total disk area in pixels of both the bark and wood was determined by counting the number of non-white pixels (<255) from one channel from the background isolated mask (Figure 2.5) (note that the masks are 3 channels since they are applied to 3 channel images). The total area in pixels of the wood was determined by counting the number of non-white pixels (<255) from one channel from the wood isolated mask. The number of bark pixels was determined by subtracting the wood area from the whole-disk area.

Inside and Outside Bark Diameters

To calculate the inside and outside bark diameters, we determined the radius of the disk in four positions from the pith measured at 90 degrees from each other. We used the bark mask image (Figure 2.6, middle image) and detected the edges by applying a canny edge detection algorithm (Canny, 1986) which returns a one-pixel-wide outline of the wood and bark edges with the edges as white (255) and the rest of the image black (0). To obtain distinct edges prior to using canny edge detection, we applied a median filter (Huang et al. 1979; Singh 2019) to the bark mask with kernel size 11 by 11, then eroded (Efford 2000; Singh 2019) the image with kernel size 7 by 7, and then dilated (Efford 2000; Singh 2019) the image using a kernel size 7 by 7. The image was then inverted so that the edges appeared black and the rest of the image appeared white. Using the X and Y coordinates of the pith (pithX and pithY), we kept either the X or Y fixed, we found those pixels for each X or Y coordinates that have black pixels. An image with these coordinates labelled is shown in Figure 2.7. Keeping the X coordinate of the pith constant, we find the top and bottom pixels that are black, and these points represent the inside and outside bark points for the top and bottom of the image. Keeping the Y coordinates of the pith constant, we find the left and right pixels that are black, and these points represent the inside and outside bark points for the left and right of the image. The distance between the coordinates of the pith and each of the eight coordinates gives four values for inside bark radius and four values for outside bark radius. Using the radius values, we calculated the two inside bark and two outside bark diameters at 90 degrees to each other and then average them together to obtain one value per property.

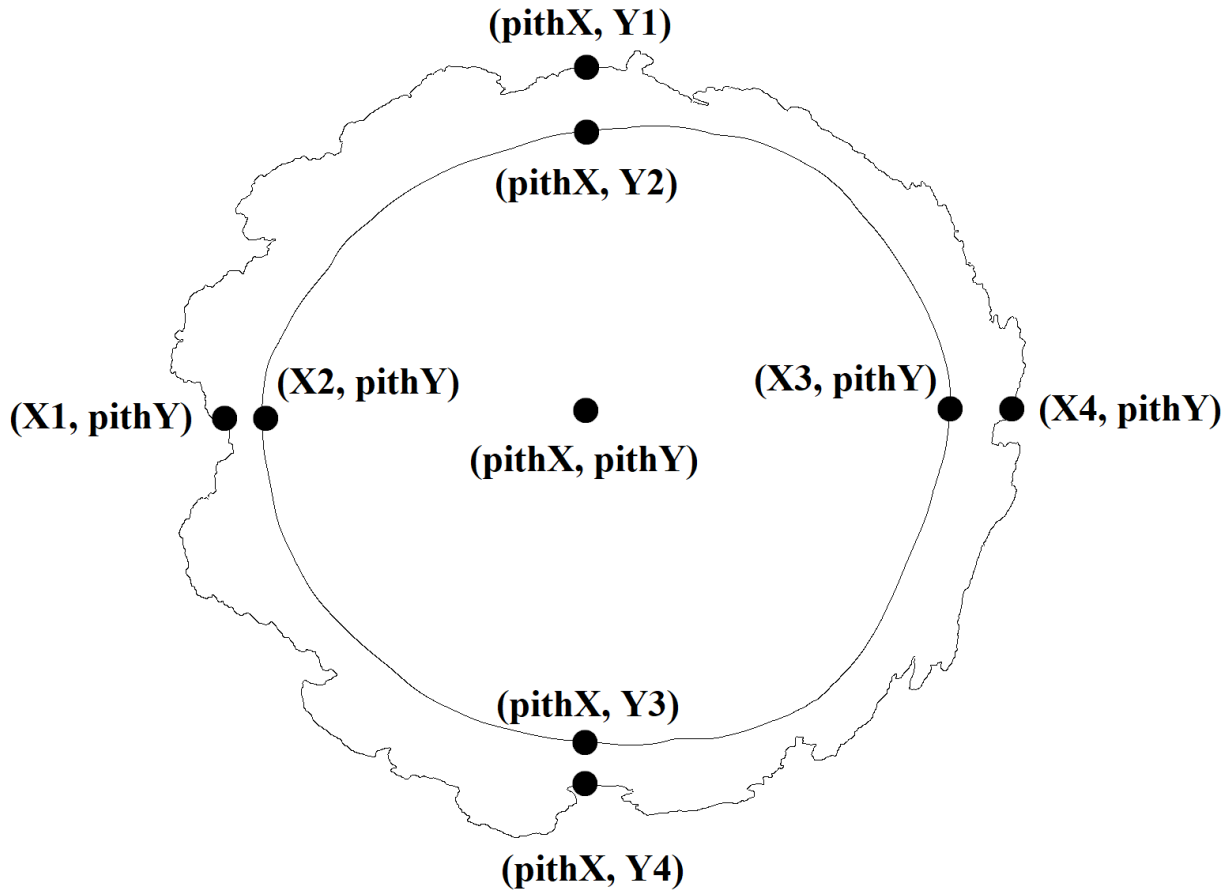

Figure 2.7. An image showing locations of points from where the coordinates were taken following canny edge detection to enable inside and outside bark diameter calculation.

Disk Shape and Compression Wood

In order to correct for vertical leaning, softwood trees produce compression wood on the underside of their stems which results in cross-sectional asymmetry (Timell 1986). Thus, eccentric radial growth and compression wood formation are often synonymous (Timell 1980). We calculated how much a disk was out of round based on the difference between the largest and smallest radius:

$$\text{Out of Round (\%)} = \frac{\text{Largest radius} - \text{Smallest radius}}{\text{Smallest radius}} \times 100$$

Disks that were out of round by 40% were classified as ‘not round’ disks and the remaining disks classified as ‘round’. The threshold of 40% was determined experimentally with the focus being to detect compression wood in disks labelled as out of round. For disks that did not exceed this 40% threshold, we found the compression wood quantification to be generally inaccurate as latewood was often labelled as compression wood in these disks.

To detect the compression wood in the out of round disks, we used the white light wood images without bark (Figure 2.6, image on the right). We converted the RGB color space to the YCrCB color space (Jack 2007):

$$\mathrm{Y} = 16 + \left(\frac{65.738\mathrm{R}}{256}\right) + \left(\frac{129.057\mathrm{G}}{256}\right) + \left(\frac{25.064\mathrm{B}}{256}\right) \quad (1)$$

$$\mathrm{Cr} = 128 + \left(\frac{112.439\mathrm{R}}{256}\right) - \left(\frac{94.154\mathrm{G}}{256}\right) - \left(\frac{18.285\mathrm{B}}{256}\right) \quad (2)$$

$$\mathrm{Cb} = 128 - \left(\frac{37.945\mathrm{R}}{256}\right) - \left(\frac{74.494\mathrm{G}}{256}\right) + \left(\frac{112.439\mathrm{B}}{256}\right) \quad (3)$$

where Y represents the brightness (luma) component, Cr and Cb represent the color difference components, and R, G, and B are the values for each pixel of the red, green, and blue channels, respectively (Jack 2007). The Cb channel (Figure 2.8, top left) shows the compression wood as being brighter than the rest of the image. We binarized the image (threshold) whereby any pixel less than 95 (determined through experimentation) was not compression wood, and any pixel greater than 95 was compression wood (Figure 2.8, top right). After converting the image to binary, we inverted the image so that compression wood was dark and normal was wood was bright. The area near the pith was falsely classified as compression wood so we removed the pith based on the coordinates of the pith. We then applied a median filter (Huang et al. 1979; Singh 2019) of kernel

size 9 by 9 to reduce noise in the image. The resultant compression wood mask is shown in Figure 2.8, bottom left.

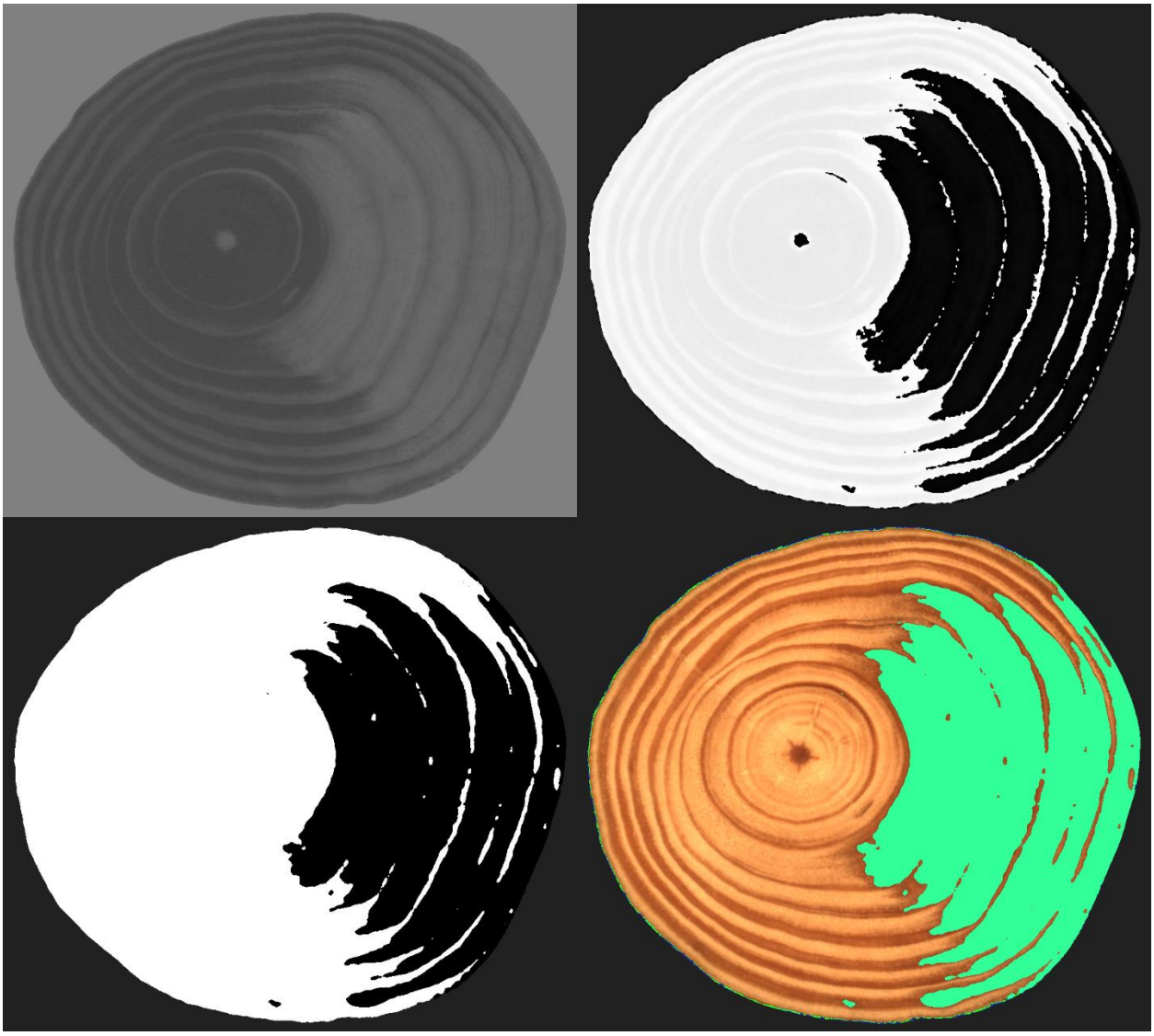

Figure 2.8. Steps involved in detection and quantification of severe compression wood using the Cb channel (top left) from the YCrCb colorspace image. Image after thresholding (top right) and image after removing the pith and applying median filter (bottom left). The identified compression wood areas then overlaid on wood only images with lime green color for visualization (bottom right image).

For illustration of compression wood, we converted the black pixels to lime green (R = 153, G = 255, and B = 51) and applied this mask to the wood images (Figure 2.8, bottom right). The images with the compression wood applied were then manually checked to determine if the technique classified the regions with severe compression wood correctly. While the focus was on applying the compression wood quantification to the 'not round' disks, images that were round were also subjected to compression wood detection and checked manually for correctness to determine how many disks that had severe compression wood were considered 'round'.

Statistical Analysis

Following the image analysis work that was done in Python (Python Software Foundation, https://www.python.org/), we saved the results to a csv file. For the remaining statistical analysis and graphics, we used R (R Core Team 2020) with the R studio interface (RStudio 2020), and the tidyverse collection of packages (Wickham and RStudio 2020) for data munging and ggplot2 (Wickham 2016) for plotting. As determined through calibration of the images to multiple reference objects of known size, each pixel represents an area of 0.000280 cm^2. As the pixels were squares, the length of each pixel was 0.0167 cm. Hence, the length and area measurements in pixels were converted to cm or cm^2. Wood and bark areas were multiplied by the height of the disk (recorded using the ultrasound sensor that positioned the disk a fixed distance from the lens) to calculate the wood and bark volumes in cm^3. Plots were made for all the volumes and diameter measurements and linear models were fitted to determine how accurate the images were to the reference measurements.

A plot showing the out of round (%) for the disks by relative height, and by ranking the disks and plotting across the rank were produced. Compression wood accuracy was determined qualitatively through visual inspection of disks. We counted the number of disks that were 'round' but still had severe compression wood, and we counted the disks that were 'not round' but the compression wood segmentation failed to accurately identify the compression wood.

2.3 RESULTS

Wood and Bark Volumes

The relationships between the reference and the image estimated wood volume measurements is shown in Figure 2.9. The two measurements were in close agreement. The fitted linear model (solid black line with intercept 8.995 and slope 0.968) had a R^2 value greater than 0.99 with a RMSE of 26.5 cm^3. The 1:1 line (dotted line) of equivalence showed that the images slightly overpredicted the wood volumes.

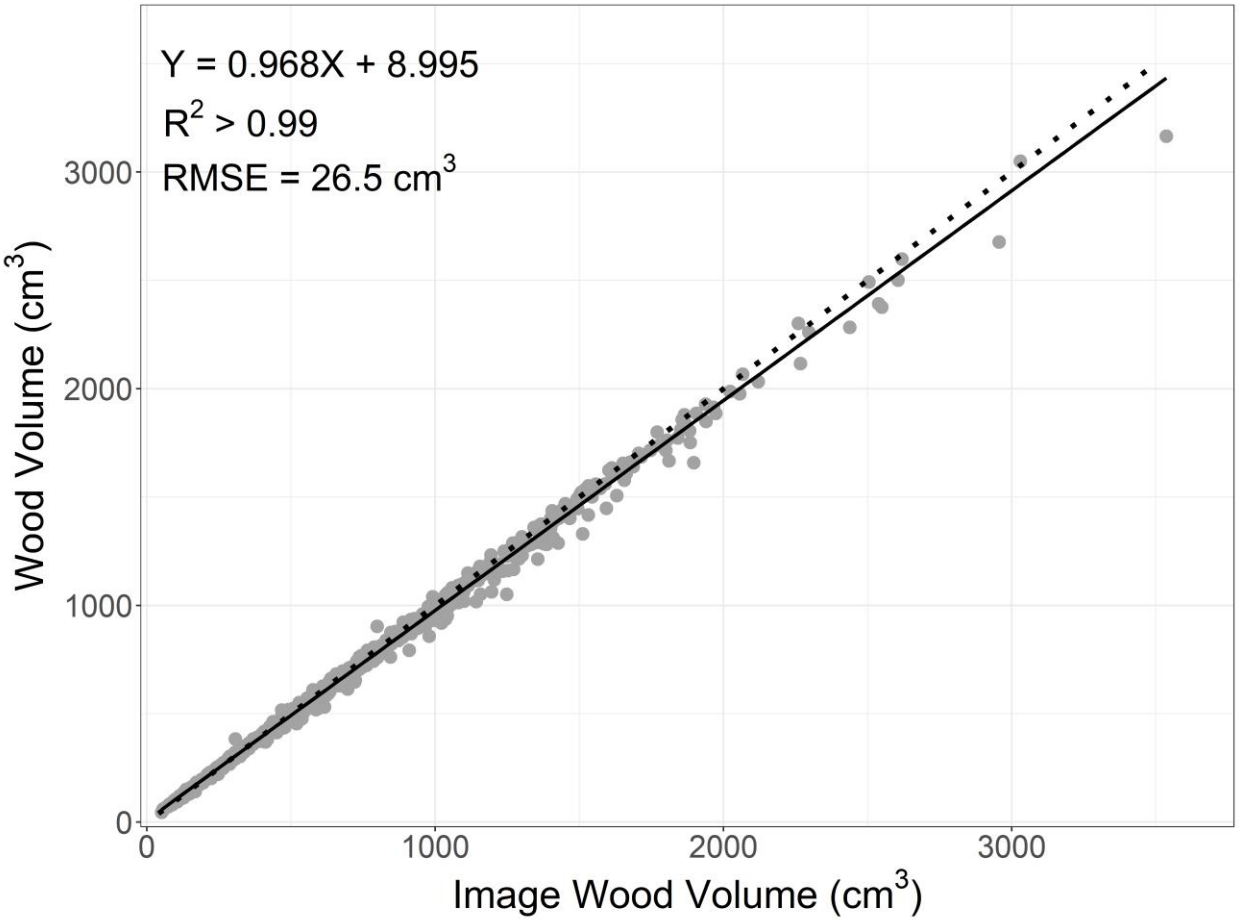

Figure 2.9. Reference wood volumes of disks plotted against the image wood volume estimates. The solid line represents the linear model fitted for the data and the dotted line represents the 1:1 line.

The relationship between the reference and the image estimated bark volume measurements is shown in Figure 2.10. Similar to the wood volume, the two bark measurements were in close agreement. The fitted linear model (solid black line with intercept 4.306 and slope 0.997) had a R^2 value of 0.96 with a RMSE of 3.9 cm^3. The 1:1 line (dotted line) of equivalence showed that the images slightly overpredicted the bark volumes.

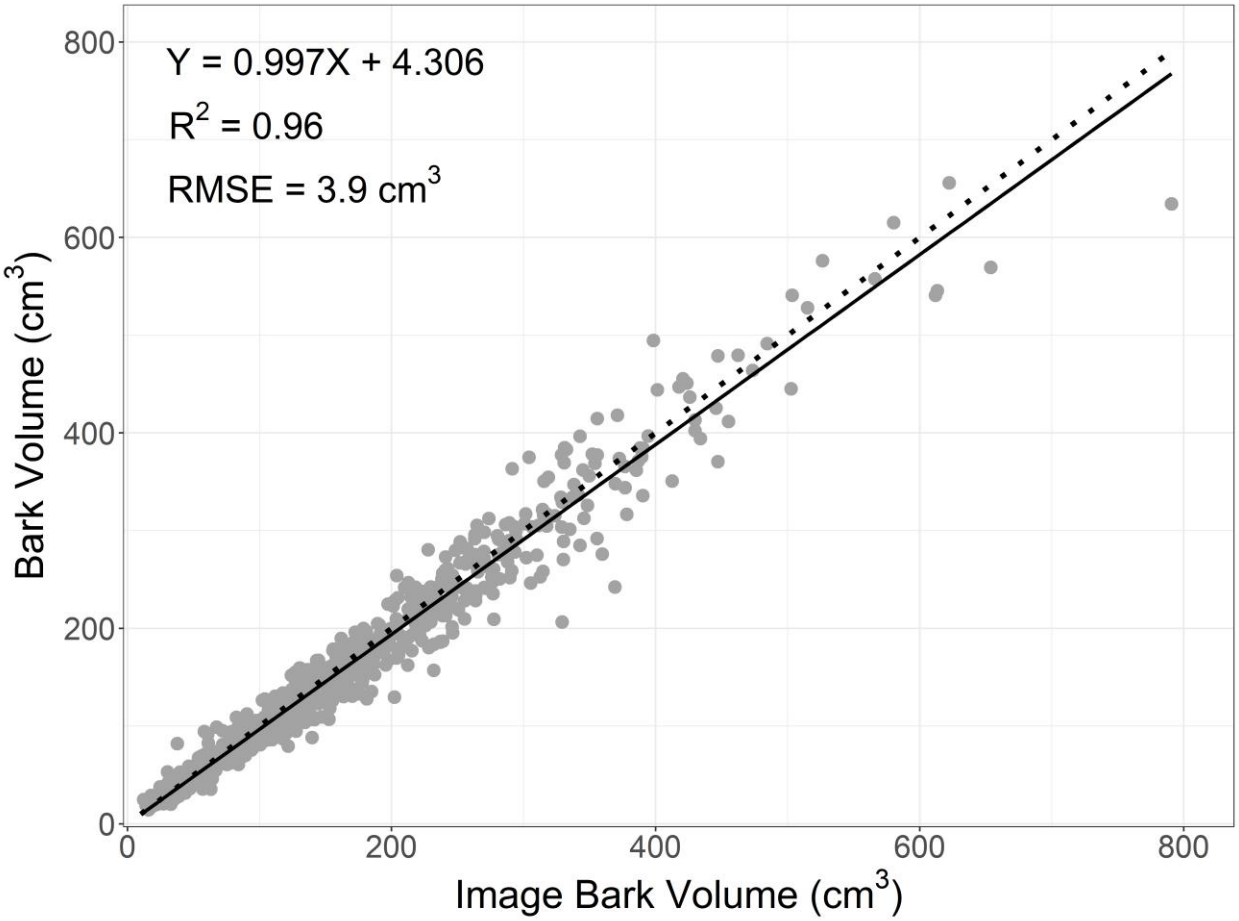

Figure 2.10. Reference bark volumes of disks plotted against the image bark volume estimates. The solid line represents the linear model fitted for the data and the dotted line represents the 1:1 line.

Outside Bark and Inside Bark Diameters

The relationships between the reference and the image estimated diameter outside bark measurements is shown in Figure 2.11. Similar to the findings on wood volume and bark volume, the two outside bark diameters measurements were in close agreement. The fitted linear model (solid black line with intercept 0.321and slope 0.959) had a R^2 value greater than 0.99 with a RMSE of 0.32 cm. The 1:1 line (dotted line) of equivalence showed that the images allowed for correct

estimates of the outside bark diameter for the disks having outside bark diameter less than 10 cm. The images slightly underpredicted the outside bark diameters, particularly as the diameter increased.

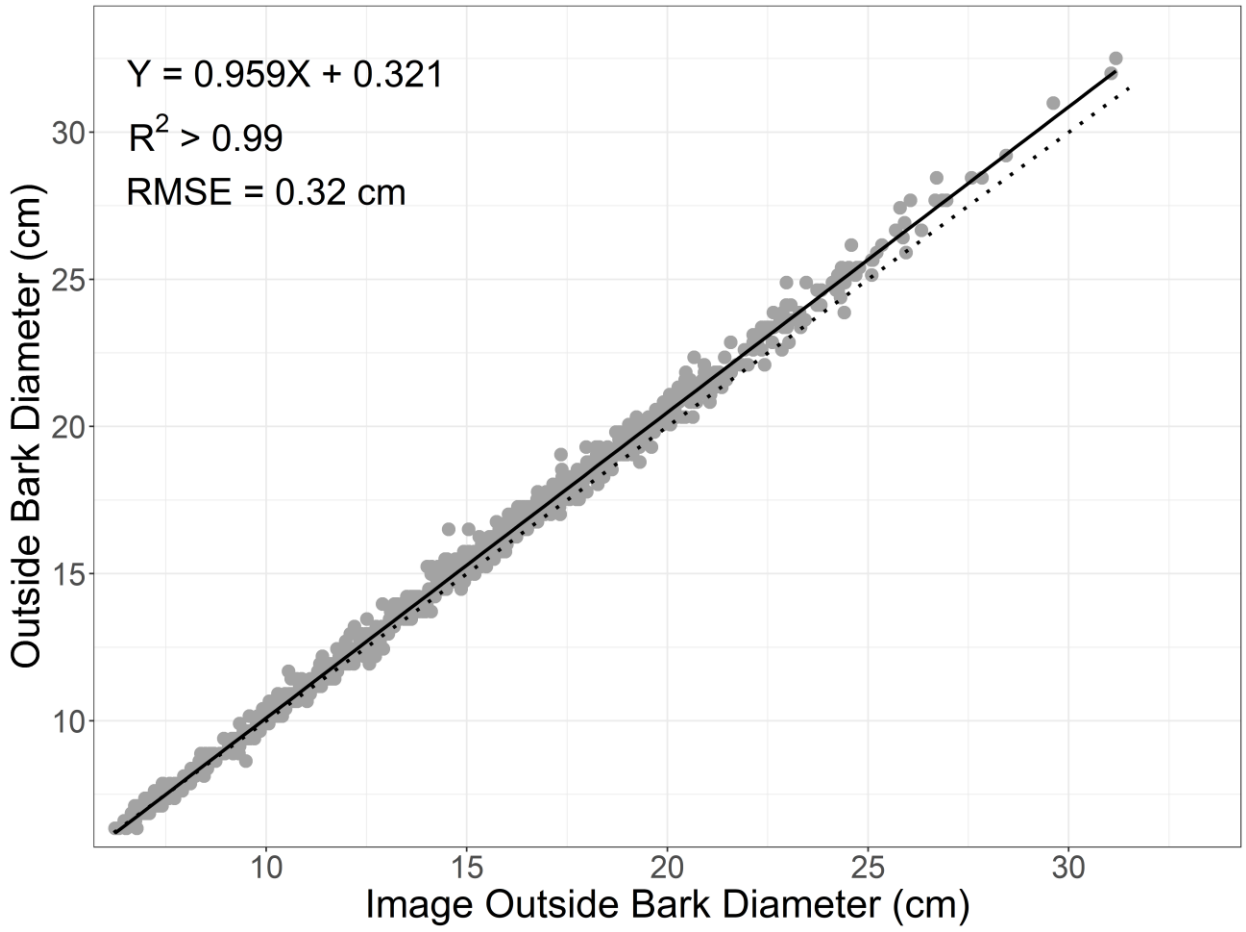

Figure 2.11. Reference outside bark diameters plotted against the image outside bark diameter estimates. The solid line represents the linear model fitted for the data and the dotted line represents the 1:1 line.

The relationships between the reference and the image estimated diameter inside bark measurements is shown in Figure 2.12. Similar to the findings on wood volume, bark volume, and outside bark diameter, the two inside bark diameters measurements were in close agreement. The fitted linear model (solid black line with intercept -0.012 and slope 0.904) had a R^2 value greater

than 0.99 with a RMSE of 0.09 cm. The 1:1 line (dotted line) of equivalence showed that there was minimal difference in the two inside bark diameter measurements.

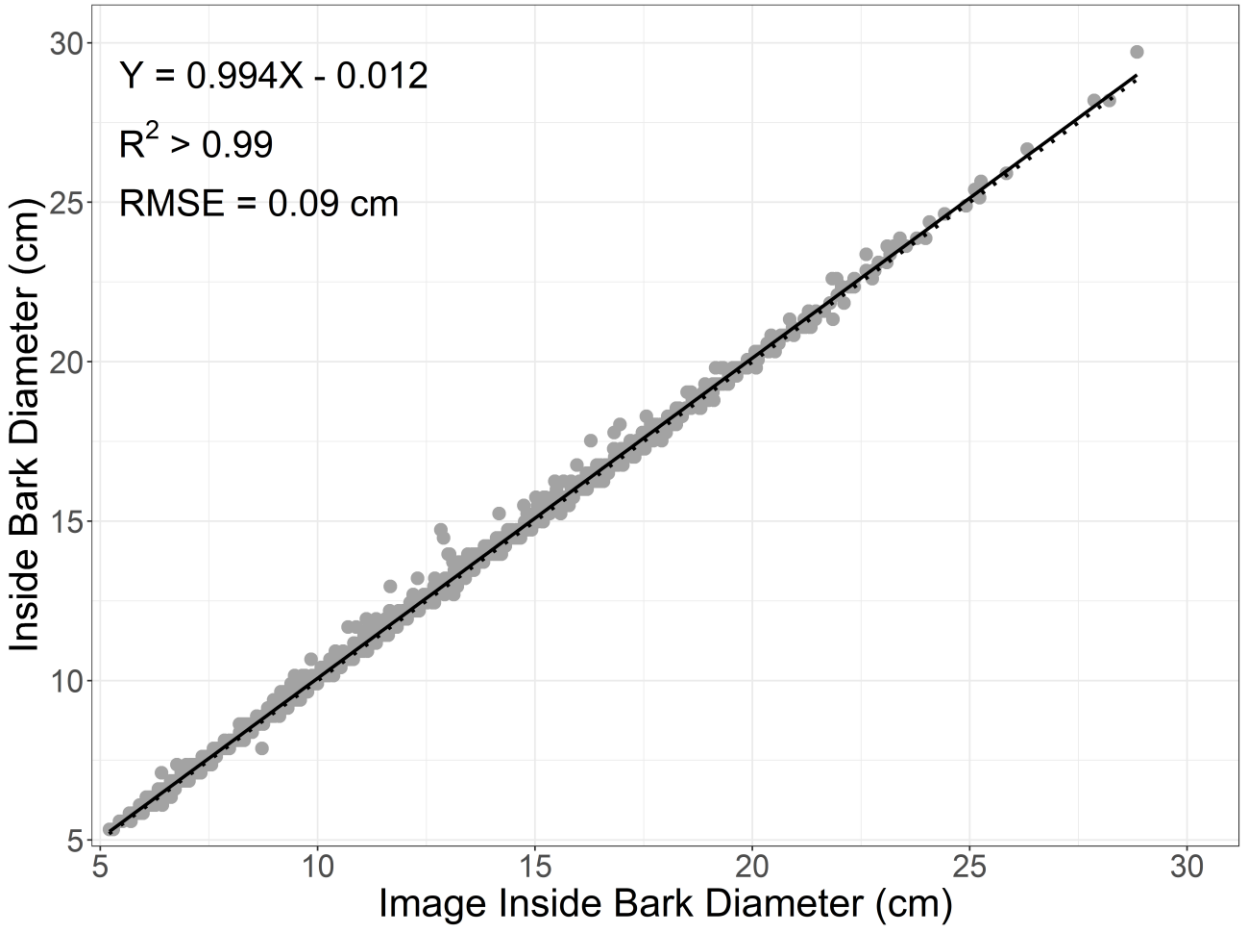

Figure 2.12. Reference inside bark diameters plotted against the image inside bark diameter estimates. The solid line represents the linear model fitted for the data and the dotted line represents the 1:1 line.

Disk Shape and Compression Wood

Using the 40% out of round threshold to determine 'not round' disks, 90 out of 1120 disks were classified as 'not round' (Table 2.2). The mean out of round value for the 'not round' disks was 77.7% (SD = 52.9%) with a range of 40.1% - 366.5%. Both smaller and larger disks were

classified as ‘not round’ with the mean inside bark diameter 12.0 cm (SD = 4.1 cm) with a range of 5.8 cm - 23.6 cm. The ‘not round’ disks were found throughout the range of relative heights, though the disks with the higher variability came from relative heights less than 0.3 (Figure 2.13). The split between ‘not round’ disks was split evenly between cutover (44 disks) and old field (46 disks) sites, however disks from cutover sites were more out of round than old field sites (Mean = 85.8%, SD = 66.0% vs Mean = 70.0%, SD = 35.2%) (Table 2.2). Out of the 90 disks classified as ‘not round’, 83 were from defect trees, so 7 disks were from non-defect trees (Figure 2.14). Hence, a total of 492 out 575 disks that came from defect trees were ‘round’.

Table 2.2. Summary of the 90 disks classified as ‘not round’ for the overall data and separated by cutover and old field sites.

	Overall (N= 90)				Cutover (N=44)				Old field (N=46)			
Property	**Mean**	**SD**	**Min**	**Max**	**Mean**	**SD**	**Min**	**Max**	**Mean**	**SD**	**Min**	**Max**
Out of round (%)	77.7	52.9	40.1	366.5	85.8	66.0	40.1	366.5	70.0	35.2	40.4	254.2
DIB (cm)	12.0	4.1	5.8	23.6	12.2	3.9	5.8	23.6	11.8	4.3	6.3	19.8

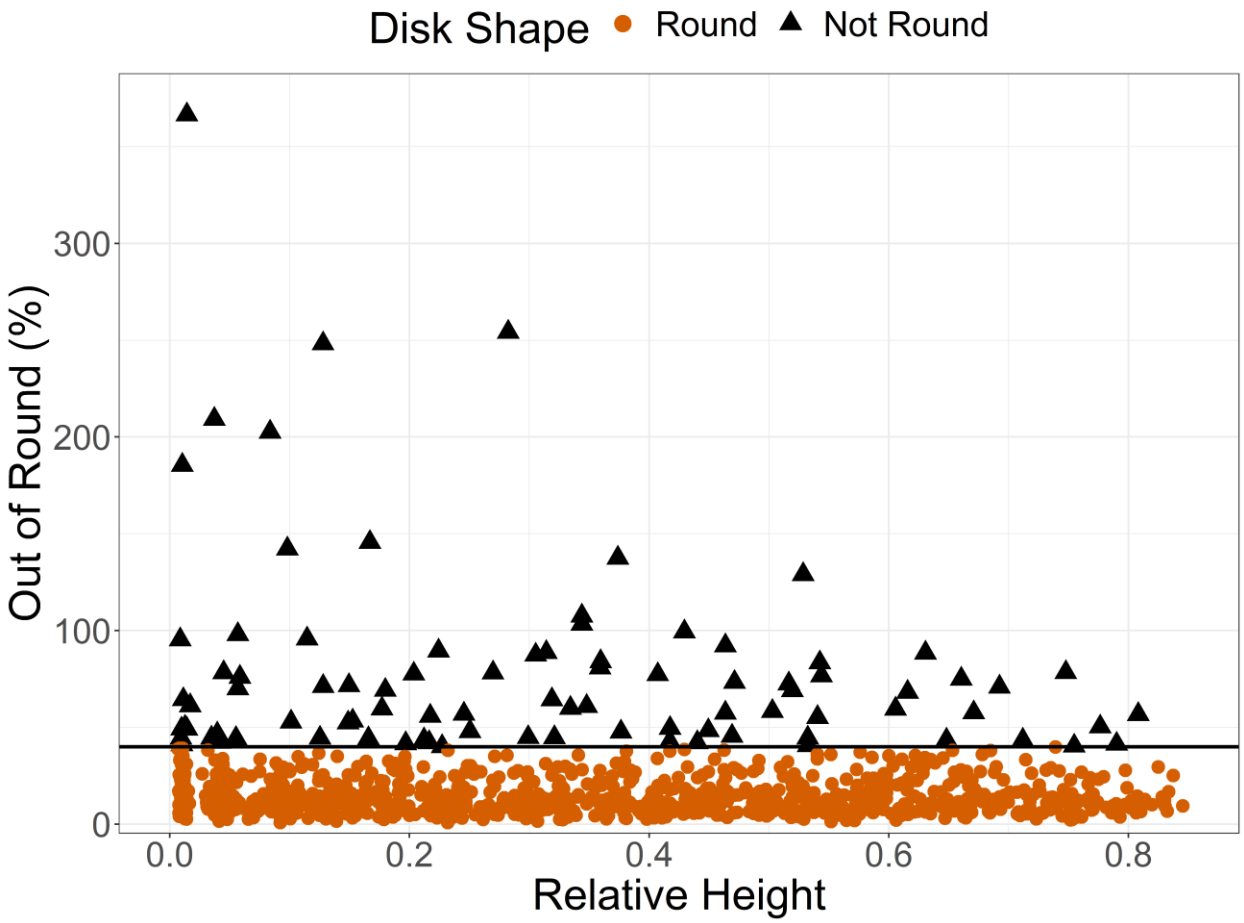

Figure 2.13. Out of round (%) plotted against relative height for all the disks. The solid black horizontal line represents the 40% threshold used to separate ‘round’ and ‘not round’ disks.

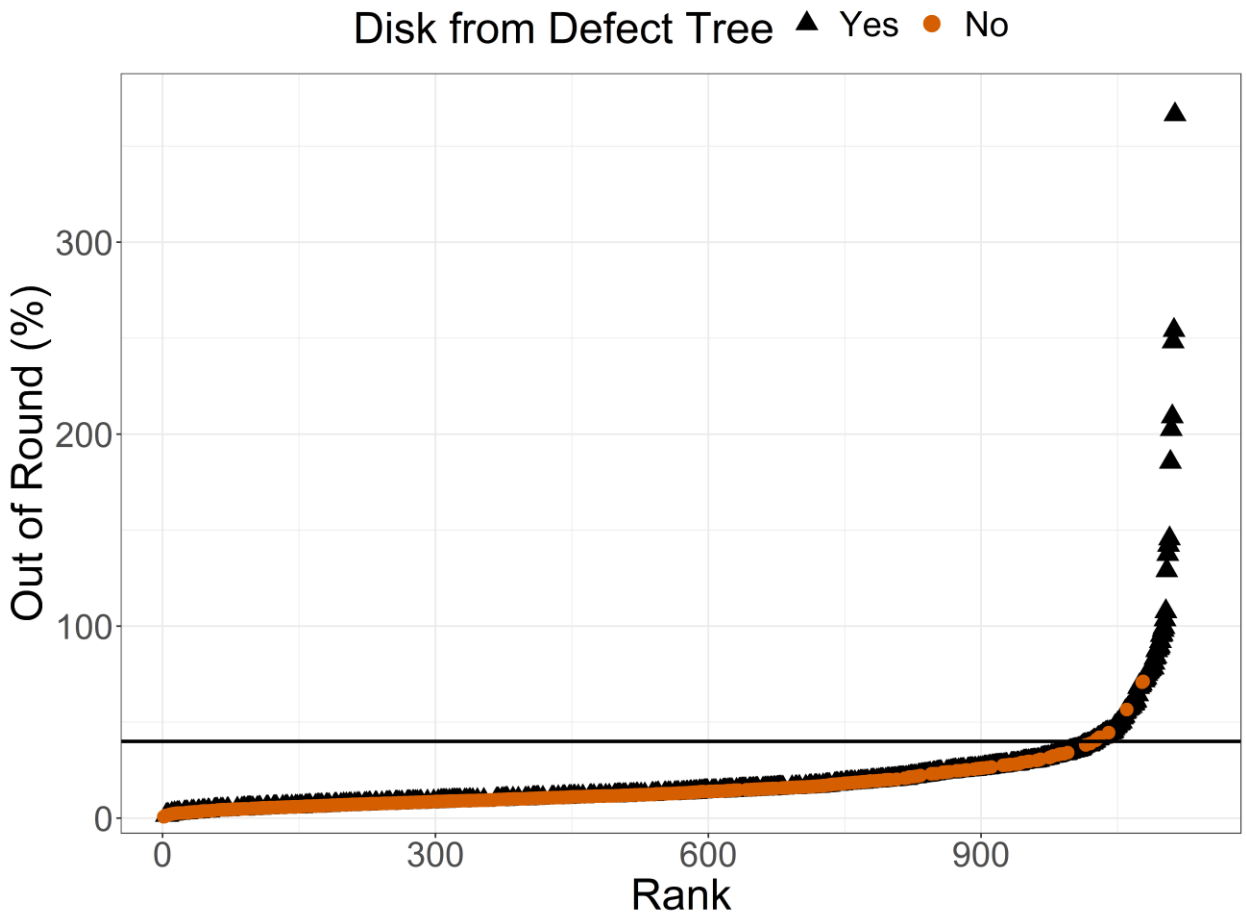

Figure 2.14. Out of round (%) plotted against a rank of itself to illustrate disks that are 'round' and 'not round' with the disks from defect and non-defect trees shown. The solid black horizontal line represents the 40% threshold used to separate 'round' and 'not round' disks.

Our method of separating the out of round disks first and then checking for severe compression wood was able to correctly classify compression wood on 61 disks out of a total of 90 disks that were classified as 'not round'. The remaining 29 disks either did not have an occurrence of severe compression wood or the latewood was falsely classified as compression wood. From the 'round' disks, 4 disks had severe compression wood but did not have a skewed pith and hence were classified as 'round'. For the 61 disks that were labelled correctly, we found

that 33.8% (SD = 16.1%) of the wood portion of the disks were composed of severe compression wood on average with a range from 6.8% to 62.3% (Table 2.3). Examining the type of tree defect types for the 61 disks that were classified as having severe compression wood, a majority of the disks came from trees that had excessive sweep (39 out of 61 disks) (Table 2.4). One average, 39.6% (SD = 16.4%) of the wood in disks from sweep trees was severe compression wood. The out of round (%) was also highest for the disks that came from trees that had excessive sweep with a mean value of 93.8% (SD = 66.4%) and a range of 40.1% - 366.5%.

Table 2.3. Summary for 61 disks classified as 'not round' that had severe compression wood (CW)

	Overall (N= 61)				**Cutover (N=32)**				**Old field (N=29)**			
Property	**Mean**	**SD**	**Min**	**Max**	**Mean**	**SD**	**Min**	**Max**	**Mean**	**SD**	**Min**	**Max**
CW as percent wood (%)	33.8	16.1	6.8	62.3	38.3	16.5	6.8	61.9	28.9	14.4	9.1	62.3
DIB (cm)	11.8	3.7	5.8	19.8	11.4	3.2	5.8	17.8	12.2	4.2	6.3	19.8

Table 2.4. Compression wood summary of 61 disks classified as 'not round' and having severe compression wood occurrence in different defect types

	Compression Wood (%)				**Out of Round (%)**			
Defect	**Mean**	**SD**	**Min**	**Max**	**Mean**	**SD**	**Min**	**Max**
Fork (N=12)	26.4	9.4	11.0	39.5	70.7	29.3	41.4	128.9
Sweep (N=39)	39.6	16.4	6.8	62.3	93.8	66.4	40.1	366.5
Mixed Defects (N=9)	19.9	8.4	9.1	37.0	70.7	24.9	43.5	107.6
None (N=1)	24.8	-	-	-	56.69			

2.4 DISCUSSION

We demonstrate using imaging to replicate reference measurements done on wood disks to calculate volume and diameter measurements. Overall, the volume and diameter results from the images provided similar results as the reference measurements determined using water displacement to calculate volume, or using a diameter tape to calculate the diameter of the disks. This was possible because of accurate camera calibration and fixed focal length. The images slightly overpredicted the wood and bark volumes. The reason for the overprediction of volume is that the disk surface is assumed smooth in the images, with equal thickness throughout the entire disk. In reality, because we only machined one surface, the bottom surface was still rough cut from the chainsaw. This uneven surface on the bottom of the disk resulted in a slight overprediction of volume. Another reason for possible differences at the individual disk level is that images are two dimensional, and the area calculated is the one imaged, and thus the imaging ignores diameter changes with height due to taper (Burkhart and Tomé 2012). Other possible sources of error are localized growth deformations on the sides of the disks which are not accounted for during imaging. In addition to biological differences within the disks themselves is the accuracy of the ultrasonic sensor and the assumption that the disks were of even thickness. It is important to note that these errors were small and imaging for wood volume had $R^2 > 0.99$. Another possible source of error is any error in the reference method, since no method is without error.

The bark volume had lower accuracy than the wood, but still high prediction accuracy ($R^2 = 0.96$). For wood volume, the volume of the wood and the image of the wood is done on the exact same piece, that is the full disk. Bark has more error because the image volume of bark is the entire bark, whereas with the reference method, the largest piece of bark is used (since bark comes off in

pieces during the peeling process), and the volume of the piece is scaled up to the full bark volume based on the weight of the bark versus the weight of the piece. Because the image represents the entire bark volume, the image measurement is likely more accurate than the work done on the piece of bark.

The measurement of diameter from the images consistently underpredicted the outside bark diameter, whereas there was almost no difference in inside bark diameter measurements. After peeling the bark from the wood, the wood surface is relatively smooth and nearly free of any fissures. Whereas with the outside bark diameter, as the disks get larger, the outer bark shape is more complicated with more fissures (Eberhardt 2015). When measuring the diameter using a diameter tape, the diameter tape is pulled tight over the fissures which overestimates the diameter slightly. With smaller disks found higher up the tree, bark thickness is more uniform all around, and we observed less differences between the reference and the image measurements. In longleaf pine, the inner bark is approximately 15% of the bark thickness at the stump height, whereas towards the top of the tree the inner bark thickness is more than 40% of the bark thickness (Eberhardt 2013). A possible discrepancy between diameter measurements was that we found the radius of the disk in 4 positions, we could have calculated the radius at more positions on a disk in an attempt to more closely predict the outside bark diameter.

A major advantage of imaging disks over the reference method is that the images enables other measurements to be collected. Here, we estimated the disk shape based on the position of the pith within the cross-section of the wood where the percentage difference between the smallest and the largest radius was calculated to determine whether a disk was ‘round’ or ‘not round’. A 40% threshold was used as to separate ‘round’ and ‘not round’ disks, a value that was determined

experimentally by examining the samples that we collected. A higher or lower threshold value can be used depending upon how much variation there is within the four radii of the sample disks used. An alternative way to detect out of roundness would be by using the idea of best fit circle as done and determining the out of roundness based on the difference between the circle of best fit and the circumference of the disk (Sauter et al. 2019). However, this method does not account for disks that are round but have a highly skewed pith which occurred here.

Using the 'out of round' disks, we also estimated the amount of the severe compression wood within the disks. We acknowledge that the compression wood measurement is an estimate. The technique only worked for severe compression wood, and our threshold of 40% to identify the 'out of round' did not always result in disks with severe compression wood. However, with the image processing steps that we used, it was relatively easy to determine if the method was working for a disk or not because we overlaid the compression wood onto the image, and then manually verified each disk for accuracy. We imaged the disks green as the compression wood in fresh disks has a darker reddish appearance which can improve accuracy in detection when using an RGB camera (Timell, 1986; Nyström and Kline, 2000). However, many researchers in the past have noted the insufficiency of an RGB camera alone to accurately detect compression wood areas (Duncker and Spiecker 2009), particularly for segmenting mild compression wood from latewood (Pont et al. 2007). Latewood specific gravity increases from pith to bark in southern pines including longleaf pine, with the latewood band of cells having lower density near the pith and these rings can be difficult to distinguish even at higher resolution (Dahlen et al. 2018). Nyström and Kline (2000) used a multivariate regression model to identify compression wood, making use of a color line scan camera and X-rays. They concluded that X-rays were not effective at

compression wood identification, however their multivariate regression model focused on color information had an accuracy of more than 87% in detecting compression wood. The relatively high accuracy of the compression wood identified by Nyström and Kline 2000) may be due to the surface imaged; they imaged lumber and thus scanned the tangential and radial surfaces of lumber, whereas we imaged the transverse surface. The amount of compression wood can be manually segmented on the disks themselves using a planimeter, or alternatively the areas can be manually segmented using image software, but both methods are extremely time consuming (Andersson and Walter 1995; Thomas 2014). We were optimistic that the fluorescence image would result in reliable separation between the latewood and the compression wood but we did not find that to be the case. Thomas (2014) found that global values for thresholding compression wood were not successful for radiata pine and we come to the same conclusion for longleaf pine. However, at an individual disk level we can distinguish mild compression wood from latewood, and thus in the future we may be able to correctly identify compression wood using a machine learning approach (Michelucci 2018; Bhuyan 2019; Singh 2019), however, a challenge is accurately labelling the compression wood. Cutting samples thin, either using a microtome, or to a few mm in thickness can result in accurate quantification of compression wood, at the expense of increased sample preparation (Andersson and Walter 1995; Thomas 2014; Thomas and Collings 2015). One approach could be to use a hyperspectral imaging system to identify the compression wood. For example Duncker and Spiecker (2009) found that hyperspectral imaging had an accuracy greater than 91% in classifying severe compression wood, moderate compression wood, normal wood, and cracks in cross-sectional disks of Norway spruce (*Picea abies*). Even though there are clear challenges with compression wood identification, the method was successful in extracting more

information than is typically attained without imaging and the measurement and verification process is relatively fast.

An additional advantage to imaging is the digital record of the image itself, which can be used for a number of purposes including comparing models generated to the actual disks, visual reference for different silvicultural treatments, as well as others. There is comparably little information available in the literature on imaging wood disks. The closest work would be the work from Scion on the DiscBot – which is a purpose-built wood quality instrument consisting of an RGB camera, a hyperspectral imaging system, acoustic velocity scanner, and an X-ray system (Schimleck et al. 2019). The DiscBot uses dry disks which are cut in half prior to drying to avoid cracking that occurs during drying due to differential shrinkage (radial shrinkage is less than tangential shrinkage). After drying, the DiscBot system captures wood property variation both radially and in circumference. Most wood and fiber quality studies looking at within tree variation collect disks from multiple height levels, but from each disk wood property variation is typically only measured radially and hence variation in circumference is not usually measured (Schimleck et al. 2019). For example, the laboratory instruments we use at the Wood and Fiber Quality laboratory at the University of Georgia are generally setup to work for radial variation and thus cannot be used on large disks. Here, using imaging on green disks, we machine the surface of the disk, image the disk, and then can process the disks as per our normal laboratory procedures. While variation due to circumference is usually ignored, Eberhardt et al. (2018) found the northern side of mature longleaf pine trees growing in the southeastern United States to have a higher ring specific gravity and higher latewood proportion as compared to the southern side.

2.5 CONCLUSION

An imaging approach was adopted to replicate reference wood and bark volume measurements made using water displacement. The results from image analysis were in close agreement with the results from the standard methods. Outside bark and inside bark diameters measured from images were also in close agreement with the measurements taken using a diameter tape. These results confirm the accuracy of the camera calibration. Imaging combined with effective surface preparation of green disks can aid in extracting accurate spatial measurements from the images. Discrepancies between the wood volume measurements were less than we found for bark volume measurements because the wood volume measurement is done on whole-disks for both the standard and imaging methods; whereas the standard bark volume measurement is done only on the largest piece obtained after peeling the bark off from the green disk and the volume of that piece is then extrapolated to the total bark volume using the bark weight. Because the image represents the entire surface of the bark, we would argue that the bark volume measurement from the image is more accurate than the reference method made using a bark piece. There was almost no difference between methods for measuring the diameter of the inside bark, whereas outside bark diameter had more variability. The outside bark surface is usually rough with fissures whereas the inside bark surface is smooth and more consistent. Four inside bark radii for each disk were used to calculate the out of round (%) with a threshold of 40% out of round to separate ‘round’ and ‘not round’ disks. Most of the ‘not round’ disks came from defect trees and were found across the entire relative height range, with trees that had excessive sweep having more ‘not round’ disks. Trees with sweep also had a higher amount of severe compression wood in them than disks from

other defect trees. We were not able to isolate mild compression wood from latewood using global parameters, thus the parameters would need to be tuned for each disk.

Acknowledgements

Funding for this research study was made possible by NRCS (project code: 68-4310-17-012). I am thankful to landowners Ben O'Conner, Chuck Fore, David Wells, Georgia Power, Heather Brassel, Joseph W. Jones Ecological Research Center at Ichauway, Lynda Beam, Lamar Zipperer, Larry Hardy, Mark Dixon, Pete Peebles, Pete Studstill, and Rayonier for allowing us to collect samples from their planted longleaf stands. I would like to thank Bryan Simmons from the Wood Quality Consortium (WQC) and my fellow graduate students Thomas Harris and Mark Porter for their help with field work and sample collection.

2.6 REFERENCES

Andersson, C., and Walter, F. 1995. Classification of compression wood using digital image analysis. For. Prod. J. **45**(11–12): 87–92.

Arbeláez, P., Maire, M., Fowlkes, C., and Malik, J. 2011. Contour detection and hierarchical image segmentation. IEEE Trans. Pattern Anal. Mach. Intell. **33**(5): 898–916. IEEE. doi:10.1109/TPAMI.2010.161.

ASTM International. 2017. D2395-17. Standard test methods for density and specific gravity (relative density) of wood and wood-based materials. ASTM International, West Conshohocken, PA. 13 p.

Beck, C.B. 2010. An introduction to plant structure and development: plant anatomy for the twenty-first century. *In* 2nd edition. Cambridge University Press, Cambridge, UK. 464 p.

Bhuyan, M.K. 2019. Computer vision and image processing: fundamentals and applications. CRC Press, Boca Raton, FL. 442 p.

Bradski, G. 2000. The OpenCV library. Dr. Dobb's J Softw Tools. **25** . 120-125.

Brüchert, F., Biechele, T., Longo, B.L., Sauter, U.H., and Pizzaro, M.E. 2019. Using X-ray computed tomography to identify wood quality parameter of high-value teak roundwood. *In* Proceedings: 21st International Nondestructive Testing and Evaluation of Wood Symposium. Gen.Tech. Rep. FPL-GTR-272. *Edited by* X. Wang, U.H. Sauter, and R.J. Ross. USDA Forest Service, Forest Products Laboratory, Madison, WI. p. 724.

Bucur, V. 2003a. Nondestructive characterization and imaging of wood. Springer, Heidelberg.

doi:10.1007/978-3-662-08986-6.

Bucur, V. 2003b. Techniques for high resolution imaging of wood structure: A review. Meas. Sci. Technol. **14**(12): R91–R98. doi:10.1088/0957-0233/14/12/R01. 354 p.

Burdon, R.D., Paul Kibblewhite, R., Walker, J.C.F., Megraw, R.A., Evans, R., and Cown, D.J. 2004. Juvenile versus mature wood: a new concept, orthogonal to corewood versus outerwood, with special reference to Pinus radiata and P. taeda. For. Sci. **50**(4): 399–415. doi:10.1139/x84-145.

Burkhart, H.E., and Tomé, M. 2012. Modeling forest trees and stands. Springer, Dordrecht, Netherlands. doi:10.1007/978-90-481-3170-9. 457 p.

Canny, J. 1986. A computational approach to edge detection. IEEE Trans. Pattern Anal. Mach. Intell. **PAMI-8**(6): 679–698. doi:10.1109/TPAMI.1986.4767851.

Dahlen, J., Auty, D., and Eberhardt, T.L. 2018. Models for predicting specific gravity and ring width for loblolly pine from intensively managed plantations, and implications for wood utilization. Forests **9**(6): 1–20. doi:10.3390/f9060292.

Decellee, R., Ngo, P., Debled-Rennesson, I., Mothe, F., and Longuetaud, F. 2019. A new algorithm to automatically detect the pith on rough log-end images. *In* Proceedings: 21st International Nondestructive Testing and Evaluation of Wood Symposium. Gen.Tech. Rep. FPL-GTR-272. *Edited by* X. Wang, U.H. Sauter, and R.J. Ross. Wang, Xiping Sauter, Udo H. Ross, Robert J., Madison, WI. p. 724.

Duncker, P., and Spiecker, H. 2009. Detection and classification of Norway spruce compression

wood in reflected light by means of hyperspectral image analysis. IAWA J. **30**(1): 59–70. doi:10.1163/22941932-90000203.

Eberhardt, T.L. 2013. Longleaf pine inner bark and outer bark thicknesses: measurement and relevance. South. J. Appl. For. **37**(3): 177–180. doi:10.5849/sjaf.12-023.

Eberhardt, T.L. 2015. Thickness and roughness measurements for air-dried longleaf pine bark. *In* Proceedings of the 17th Biennial Southern Silvicultural Research Conference. e-Gen. Tech. Rep. SRS-203. *Edited by* A.G. Holley, K.F. Connor, and J.D. Haywood. USDA Forest Service, Southen Research Station, Asheville, NC. pp. 374–379.

Eberhardt, T.L., Dahlen, J., and Schimleck, L. 2017. Species comparison of the physical properties of loblolly and slash pinewood and bark. Can. J. For. Res. **47**(11): 1495–1505. doi:10.1139/cjfr-2017-0091.

Eberhardt, T.L., So, C.L., and Leduc, D.J. 2018. Wood variability in mature longleaf pine: Differences related to cardinal direction for a softwood in a humid subtropical climate. Wood Fiber Sci. **50**(3): 1–14.

Efford, N. 2000. Digital image processing: A practical introduction using Java. *In* 1st edition. Addison-Wesley Longman Publishing Co., Inc., Boston, MA. doi:10.1049/ep.1978.0474.

Evans, R. 1994. Rapid measurement of the transverse dimensions of tracheids in radial wood sections from pinus radiata. Holzforschung **48**(2): 168–172. doi:10.1515/hfsg.1994.48.2.168.

Evans, R., Hughes, M., and Menz, D. 1999. Microfibril angle variation by scanning X-ray

diffractometry. Appita J. **52**: 363–367.

Habite, T., Olsson, A., and Oscarsson, J. 2019. Detection of pith location of Norway spruce timber boards on the basis of optical scanning. *In* Proceedings: 21st International Nondestructive Testing and Evaluation of Wood Symposium. Gen.Tech. Rep. FPL-GTR-272. *Edited by* X. Wang, U.H. Sauter, and R.J. Ross. USDA Forest Service, Forest Products Laboratory, Madison, WI. p. 724.

Huang, T.S., Yang, G.J., and Tang, G.Y. 1979. A fast two-dimensional median filtering algorithm. IEEE Trans. Acoust. **27**(1): 13–18. doi:10.1109/TASSP.1979.1163188.

Jack, K. 2007. Video demystified: A handbook for the digital engineer. *In* 5th edition. Newnes, Newton, MA. 944p.

Megraw, R.A. 1985. Wood quality factors in loblolly pine: The influence of tree age, position in tree, and cultural practice on wood specific gravity, fiber length, and fibril angle. TAPPI Press, Peachtree Corners, GA, USA. 88 p.

Michelucci, U. 2018. Advance applied deep learning. Springer, New York, NY. doi:10.1007/978-1-4842-3790-8. 410 p.

Nyström, J. 2003. Automatic measurement of fiber orientation in softwoods by using the tracheid effect. Comput. Electron. Agric. **41**(1–3): 91–99. doi:10.1016/S0168-1699(03)00045-0.

Nyström, J., and Kline, D.E. 2000. Automatic classification of compression wood in green southern yellow pine. Wood Fiber Sci. **32**(3): 301–310.

Oliphant, T.E. 2006. A guide to NumPy. Trelgol Publishing, USA. 85 p.

Papari, G., and Petkov, N. 2011. Edge and line oriented contour detection: state of the art. Image Vis. Comput. **29**(2–3): 79–103. Elsevier B.V. doi:10.1016/j.imavis.2010.08.009.

Pont, D., Brownlie, R.K., and Grace, J.C. 2007. Disc image-processing software for three-dimensional mapping of stem ring width and compression wood. New Zeal. J. For. Sci. **37**(2): 169–185.

R Core Team. 2020. R: A language and environment for statistical computing. R Foundation for Statistical Computing, Vienna, Austria. Available from URL https://www.R-project.org/ [accessed 3 April 2020].

Riddell, M., Cown, D., Harrington, J., Lee, J., and Moore, J. 2012. Assessing spiral grain angle by light transmission- Proof of concept. IAWA J. **33**: 1–14. doi:10.1163/22941932-90000075.

Roblot, G., Bléron, L., Mériaudeau, F., and Marchal, R. 2010. Automatic computation of the knot area ratio for machine strength grading of Douglas-fir and Spruce timber. Eur. J. Environ. Civ. Eng. **14**(10): 1317–1332. doi:10.3166/ejece.14.1317-1332.

Ross, R.J. 2015. Nondestructive testing and evaluation of wood. *In* Nondestructive evaluation of wood: Second edition. Gen. Tech. Rep. FPL-GTR-238. *Edited by* R.J. Ross. USDA Forest Service, Forest Products Laboratory, Madison, WI. 169 p.

Ross, R.J., and Pellerin, R.F. 1994. Nondestructive testing for assessing wood members in structures: A review. Gen. Tech. Rep. FPL-GTR-70. USDA Forest Service, Forest Products Laboratory, Madison, WI. 167 p.

RStudio. 2020. RStudio: integrated development for R. RStudio, Inc., Boston, MA. Available from URL http://www.rstudio.com/ [accessed 3 April 2020].

Sauter, U.H., Staudenmaier, J., and Huber, M. 2019. High-precision determination of round wood diameters and cross-section areas. *In* Proceedings: 21st International Nondestructive Testing and Evaluation of Wood Symposium. Gen.Tech. Rep. FPL-GTR-272. *Edited by* X. Wang, U.H. Sauter, and R.J. Ross. Wang, Xiping Sauter, Udo H. Ross, Robert J., Madison, WI. p. 724.

Schimleck, L., Dahlen, J., Apiolaza, L.A., Downes, G., Emms, G., Evans, R., Moore, J., Pâques, L., Van den Bulcke, J., and Wang, X. 2019. Non-destructive evaluation techniques and what they tell us about wood property variation. Forests **10**(9). doi:10.3390/f10090728.

Singh, H. 2019. Practical machine learning and image processing. Springer, New York, NY. doi:10.1007/978-1-4842-4149-3. 169 p.

Thomas, J. 2014. An investigation on the formation and occurrence of spiral grain and compression wood in radiata pine (*Pinus radiata* D . Don .). Doctoral Thesis, School of Biological Sciences, University of Canterbury, Christchurch, New Zealand.

Thomas, J., and Collings, D.A. 2015. Three-dimensional visualization of spiral grain and compression wood in *Pinus Radiata* imaged by circular polarized light and fluorescence. Wood Fiber Sci. **48**: 22–27.

Thomas, R.E., and Bennett, N.D. 2014. Accurately determining log and bark volumes of saw logs using high-resolution laser scan data. *In* Proceedings of the 19th Central Hardwood

Forest Conference. GTR-NRS-P-142. *Edited by* J.W. Groninger, E.J. Holzmueller, C.K. Nielsen, and D.C. Dey. USDA Forest Service, Northern Research Station, Carbondale, IL. pp. 299–310.

Timell, T.E. 1980. Karl Gustav Sanio and the first scientific description of compression wood. IAWA J. **1**(4): 147–153.

Timell, T.E. 1986. Compression wood in gymnosperms. Springer-Verlag, Berlin ; New York. 2150 p.

Wickham, H. 2016. ggplot2: elegant graphics for data analysis. Springer-Verlag, New York, NY. 260 p.

Wickham, H., RStudio. 2020. tidyverse: easy install and load the "tidyverse". R package version 1.3.0. Available from URL https://CRAN.R-project.org/package=tidyverse [accessed 3 April 2020]

Wright, S., Dahlen, J., Montes, C., and Eberhardt, T.L. 2019. Quantifying knots by image analysis and modeling their effects on the mechanical properties of loblolly pine lumber. Eur. J. Wood Wood Prod. **77**(5): 903–917. Springer Berlin Heidelberg. doi:10.1007/s00107-019-01441-8.

Yadav, A., Anand, R.S., Dewal, M., and Gupta, S. 2017. Binary wavelet transform-based completed local binary pattern texture descriptors for classification of microscopic images of hardwood species. Wood Sci. Technol. **51**: 909–927. doi:10.1007/s00226-017-0902-0.